Original Article

MOLECULAR METABOLISM

Histone H3K9 butyrylation is regulated by dietary fat and stress via an Acyl-CoA dehydrogenase short chain-dependent mechanism

Zhi Yang [1], Minzhen He [1], Julianne Austin [1], Jessica Pfleger [2], Maha Abdellatif [1,*]

ABSTRACT

Objective: We previously reported that β-oxidation enzymes are present in the nucleus in close proximity to transcriptionally active promoters. Thus, we hypothesized that the fatty acid intermediate, butyryl-CoA, is the substrate for histone butyrylation and its abundance is regulated by acyl-CoA dehydrogenase short chain (ACADS). The objective of this study was to determine the genomic distribution of H3K9-butyryl (H3K9Bu) and its regulation by dietary fat, stress, and ACADS and its impact on gene expression.

Methods and results: Using genome-wide chromatin immunoprecipitation-sequencing (ChIP—Seq), we show that H3K9Bu is abundant at all transcriptionally active promoters, where, paradoxically, it is most enriched in mice fed a fat-free vs high-fat diet. Deletion of fatty acid synthetase (FASN) abolished H3K9Bu in cells maintained in a glucose-rich but not fatty acid-rich medium, signifying that fatty acid synthesis from carbohydrates substitutes for dietary fat as a source of butyryl-CoA. A high-fat diet induced an increase in ACADS expression that accompanied the decrease in H3K9Bu. Conversely, the deletion of ACADS increased H3K9Bu in human cells and mouse hearts and reversed high-fat- and stress-induced reduction in promoter-H3K9Bu, whose abundance coincided with diminished stress-regulated gene expression as revealed by RNA sequencing. In contrast, H3K9-acetyl (H3K9Ac) abundance was minimally impacted by diet.

Conclusion: Promoter H3K9 butyrylation is a major histone modification that is negatively regulated by high fat and stress in an ACADS-dependent fashion and moderates stress-regulated gene expression.

Key words butyrylation; H3K9Bu; ACADS; Cardiac hypertrophy; Epigenetics; H3K9Ac

1. INTRODUCTION

Some TCA cycle intermediates are required for histone modifications. For example, citrate is exported from the mitochondria and converted into acetyl-CoA via nuclear ATP citrate lyase [1]. Alternatively, acetyl-CoA can be synthesized from pyruvate via pyruvate dehydrogenase complex present in the nucleus [2,3]. Similarly, oxoglutarate dehydrogenase has also been located in the nucleus in association with chromatin [4], where it supplies succinyl-CoA for histone succinylation [5]. We recently identified β-oxidation enzymes assembled in the nucleus at H2A.Z-occupied promoters [4], which led us to hypothesize that they are potentially a source of short-chain acyl-CoA moieties in the nucleus required for histone modifications.

Histone acetylation and methylation are associated with transcriptional regulation, where increases in specific histone K-acetylation are generally associated with actively transcribed genes and enhanced transcriptional activity, while methylation has a more differential effect depending on the histone, residue, and number of methyl moieties added [6]. These modifications influence transcription partly by regulating the accessibility and binding of transcription factors to the promoters and regulatory elements of genes in a highly specific fashion. In contrast, the roles of other histone modifiers remain ambiguous, as functional studies are in their early stages. Specifically, with regard to histone butyrylation, it was first identified by Chen et al., in 2007 by mass spectrometry of H4 [7]. It has since been studied in sperm, where H4K5 butyrylation competes with acetylation of the same Lys residue and inhibits the binding of Brdt [8]. In the liver, starvation-induced ketogenesis increased pan histone H3 butyrylation [9], while in a high-fat diet-induced obesity model, H3K18Bu was downregulated [10]. There are potentially two sources of butyryl-CoA in the cell. The first is its production as an intermediate of the β-oxidation spiral of even-chain fatty acids. The second is its synthesis from butyrate (produced in the intestine by bacterial fermentation of non-digestible polysaccharides) via acyl-CoA synthetase short-chain family member 2 (ACSS2) in the nucleus [11]. The latter is considered the more likely source, as butyryl-CoA produced via β-oxidation cannot be exported from the mitochondria unless plausibly if converted into butyrylcarnitine when in excess, although it remains uncertain how the latter is exported from the mitochondria [12].

ACADS is an enzyme that reduces butyryl-CoA to crotonyl-CoA in the last steps of the β-oxidation spiral [12]. Therefore, the accumulation of butyryl-CoA during β-oxidation and, accordingly, histone butyrylation

[1]Department of Cellular Biology and Molecular Medicine, Rutgers University-New Jersey Medical School, Newark, NJ, 07103, USA [2]Center for Translational Medicine, Temple University, Philadelphia, PA, 19140, USA

*Corresponding author. E-mail: abdellma@njms.rutgers.edu (M. Abdellatif).

Received February 4, 2021 • Revision received April 30, 2021 • Accepted May 6, 2021 • Available online 11 May 2021

https://doi.org/10.1016/j.molmet.2021.101249

will depend on the activity/abundance of this enzyme. In this study, we show that H3K9Bu is enriched at the promoters of all expressed genes in the heart and decreases dramatically by high dietary fat, which increases ACADS, or by stress, which is reversed by deletion of ACADS. In the absence of fatty acids, acetyl-CoA produced from glucose is converted into fatty acid by FASN [13], which is required for H3K9 butyrylation under this condition. Higher levels of promoter-H3K9Bu are associated with moderated stress-regulated gene expression, as seen with the low- vs. high-fat diet or in ACADS-deleted mice vs wild-type mice.

2. MATERIALS AND METHODS

2.1. Animals, diets, and animal care

Ten- to 12-week-old C57BL/6J, Balc/cJ, and Balb/cByJ mice were purchased from the Jackson Laboratory. Mice diets were purchased from Research Diets, Inc. (New Brunswick, NJ, USA), including a custom-made 0 Kcal % fat, 80 Kcal % carbohydrate, 20 Kcal % protein diet (fat-free, cat# D10062804Gi); 10 Kcal % fat, 70 Kcal % carbohydrate, 20 Kcal % protein diet (low-fat, cat# D12450B); and 60 Kcal % fat, 20 Kcal % carbohydrate, 20 Kcal % protein diet (high-fat, cat# D12492). Sprague–Dawley dams with 1- to 2-day-old pups were purchased from Envigo (Indianapolis, IN, USA). All the animal procedures used in this study were in accordance with the US National Institute of Health's Guidelines for the Care and Use of Laboratory Animals (No. 85–23). All the protocols were approved by the Institutional Animal Care and Use Committee at the Rutgers-New Jersey Medical School.

2.2. Human haploid (Hap1) and Hap1 knockout cell lines

Hap1, Hap1Δacetyl-CoA acyltransferase 2 (ΔACAA2), Hap1Δhydroxyacyl-CoA dehydrogenase A (ΔHADHA), Hap1ΔFASN, and Hap1ΔACADS cell lines were purchased from Horizon Discovery and cultured in Dulbecco's Modified Eagle Medium (DMEM) with 10% fetal bovine serum (FBS). These cells were fibroblast-like derived from human male chronic myelogenous leukemia (CML) cell line KBM-7. The knockouts were generated by CRISPR/Cas9 editing of the genes as follows: Hap1ΔACAA2 was generated by an 8 bp deletion in exon 6, Hap1ΔHADHA was generated by a 7 bp deletion in exon 14, Hap1ΔFASN had a 2 bp insertion in exon 42, and Hap1ΔACADS was generated by a 19 bp deletion in exon 5. All the lines were viable and proliferated at relatively normal rates, except the Hap1ΔFASN and Hap1ΔACADS were smaller in size relative to the parent cell line.

2.3. Culturing neonatal cardiac myocytes

Cardiac myocytes were cultured as described in our previous reports [14]. Briefly, hearts were isolated from 1-day-old Sprague–Dawley rats. After dissociation with collagenase, cells were subjected to Percoll gradient centrifugation followed by differential pre-plating for 30 min to enrich cardiac myocytes and deplete non-myocyte cells. Myocytes were cultured in DMEM/F12 plus 10% fetal bovine serum (FBS).

2.4. Construction of GFP fusion ACADS and NLS mutant

Plasmids harboring cDNAs of turbo-GFP (tGFP) and mouse ACADS (NM_007383) were purchased from Origene. The latter's cDNA was then subcloned in-frame upstream of tGFP and the fusion cDNA was subsequently subcloned into pDC316 shuttle plasmid vector (Microbix), which was used to generate recombinant adenoviral vectors via homologous recombination in HEK293. NLS-mutant ACADS cDNA was generated by a polymerase chain reaction-based approach that substituted lysine 335, 338, and 339 for glutamine.

2.5. Construction and delivery of recombinant adenovirus (Ad) vector

Recombinant adenoviral vectors were constructed, propagated, purified, and tittered as described in our previous reports [15–17]. Briefly, cDNA was cloned into the pDC316 shuttle vector (Microbix Biosystems Inc.) downstream of a cytomegalovirus (CMV) promoter. These were co-transfected with replication-defective human adenovirus serotype 5 (Ad5) viral DNA backbone into 293HEK cells, where a Cre-Lox-mediated recombination reaction introduced the cDNA insert into the viral DNA. Single virus plaques were amplified in 293HEK cells, purified on a cesium chloride gradient, dialyzed, and tittered on 293HEK cells with an agarose overlay. Cardiac myocytes were infected with 10–30 multiplicity of infection (moi) of the viruses for ~20 h.

2.6. Recombinant modified nucleosomes, subcellular fractionation, and Western blotting

Recombinant nucleosomes with modified histones H3K9Ac (cat# 16-0314), H3K9Bu (cat# 16-0371), and H3K18Bu (cat# 16-0373) were purchased from EpiCypher, Inc., and analyzed by Western blotting with the corresponding antibodies.

Cellular protein (25-50 μg) was fractionated using a subcellular protein fractionation kit (Thermo Fisher Scientific, cat# 78,840) according to the manufacturer's protocols. The cellular fractions were separated on a 4%–12% gradient SDS-PAGE (Criterion gels, Bio-Rad) and transferred to nitrocellulose membranes. The antibodies used included anti-H3K9Bu (Abcam, cat# ab241248), anti-H3K18Bu (PTM Bio, cat# PTM-331), anti-H3K9-crotonyl (RevMab, cat# 31-1225,099), anti-H3K27-b-hydroxybutyryl (Abcam, cat# ab241463), anti-H3K9-b-hydroxybutyryl (Thermo Fisher Scientific, PIPA5112503), anti-ACADS (Origene, cat# TA321036), anti-ACAA2 (Origene, cat# TA506126), anti-ACC1/2 (Cell Signaling Technology, cat# 36,765), anti-FASN (Abcam, cat# ab22759), anti-H3 (Active Motif, cat# 61,476), anti-H3K9Ac (Active Motif, cat# 39,917), anti-AKT1 (Millipore 07-416), anti-voltage-dependent anion-selective channel 1 (VDAC1, Genscript, cat# A01419), anti-RNA pol II (Active Motif, cat# 102,660), and anti-turboGFP (Origene, cat# TA150041). Western blotting signals were detected by an Odyssey imaging system (LI-COR) and quantitated using ImageJ.

2.7. Mitochondrial stress test

This was performed as previously described [18]. Hap1 or Hap1ΔFASN were seeded in 96-well Seahorse analyzer plates (50,000 cells/well) in full medium DMEM plus 10% FBS overnight (~20 h). The medium was then changed to DMEM (with 17.5 mM of glucose) without FBS (since it contained fatty acids) or DMEM (glucose-free) without FBS plus 100 μM of palmitate bovine serum albumin (BSA) as indicated in Figure 4. Using a Seahorse XF^{e}96 Analyzer, basal oxygen consumption rates (OCR) were measured in live cells followed by measurements after the sequential addition of 1 μM of oligomycin 8 min after the start of measurements, 1 μM of FCCP at 22 min, and 10 μM of anti-mycin A plus rotenone at 35 min. Two or 3 readings were taken after each compound was injected, and the results were plotted in real time in *p*mol/min vs time (min) [19]. The raw data were then exported to an Agilent Seahorse XF Mito Stress Test Report Generator file to calculate and graph the mitochondrial basal capacity, spare respiratory capacity, proton leak, and ATP production.

2.8. Transverse aortic constriction (TAC) in mice

This was performed as described in our previous reports [20,21]. Briefly, a 7-0 braided polyester suture was tied around the transverse

thoracic aorta against a 27-gauge needle between the innominate artery and left common carotid artery. Control mice were subjected to a sham operation involving the same procedure minus the aortic constriction.

2.9. Echocardiography and Doppler measurements

This was performed as described in our previous reports [20,21]. Briefly, transthoracic echocardiography was performed using a Vevo 3100 imaging system (Visual Sonics, Inc.) with a MX400-30 MHz (mouse cardiology) scan head encapsulated transducer. Electrocardiographic electrodes were taped to the four paws, and then, one-dimensional (1D) M mode and 2D B mode tracings were recorded from the parasternal short-axis view at the mid papillary muscle level. Pulse-wave Doppler was used to measure the blood flow velocity and peak gradient pressure in the aorta. For analysis, we used Vevo 3100 Software (Vevo Lab v3.2.6), which included analytic software package for B mode (2D) image capture and analysis; cine loop image capture, display, and review; software analytics for advanced measurements and annotations; and physiological data on-screen tracing.

2.10. ChIP—seq analysis (Active Motif)

The mice were subjected to transverse aortic constriction or a sham operation. After 7 days, cardiac function and structures were assessed by echocardiography before isolation of the hearts. Mice heart tissues were then analyzed by ChIP using the following antibodies: anti-H3K9Bu (Abcam, cat# ab241248), anti-H3K9-acetyl (H3K9Ac) (Active Motif, cat# 39,918), and anti-ACAA2 (Origene Technologies, cat# TA506126) followed by next-generation sequencing (Active Motif). Briefly, ChIP libraries ($\sim$200 bp average fragment length) were sequenced using NextSeq 500, generating 75 nt single-end sequence reads that were mapped to the genome using BWA algorithms. The reads/tags were extended *in silico* by 200 bp at their 3′end (fragments), the density of which was determined along the genome divided into 32 nt bins. The results were saved in BigWig and binary alignment/map (BAM) files, which were used for the plots, heatmaps, and images of the fragments aligned to the chromosome coordinates. Fragment peaks were identified using MACS [22] (for ACAA2 ChIP—Seq and histone marks), which identified local areas of tag enrichment compared to input, defined as intervals, while overlapping intervals were grouped into merged regions. The locations and proximities to gene annotations of the intervals and active regions were defined and compiled in Excel spreadsheets, which included average and peak fragment densities. The number of peaks in each sample and the fraction of reads in peaks (FRiP) values are included in the Results section and tabulated in Supplementary Table 1S.

We also analyzed the fragment densities by gene region, where the average value (Avg Val) of fragment densities at the transcription start site (TSS, $-$1,000 to $+$1,000) and gene bodies ($+$1,000 to 3' end) regions for all of the genes were calculated separately. These results were integrated with those of the RNA-Seq data, which were used to sort the genes into upregulated, downregulated, or unchanged after transverse aorta constriction.

2.11. RNA-seq analysis (Active Motif)

Using an Illumina NextSeq 500, 42 nt sequence reads were generated, which were aligned with the genome using the STAR algorithm. Read pairs that had both ends aligned were counted, and those with at least 25 bp overlapping bases in a fragment were assigned. Gene annotations were obtained from the Subread package [23]. Differential genes were detected by DESeq2 at 10%FDR (adjusted p value) [24].

2.12. ChIP—seq and RNA-Seq analysis software

An integrated genome browser [25] can be downloaded for free at http://bioviz.org/igb/, EaSeq [26] can be downloaded for free at http://easeq.net/, and GSEA can be downloaded for free at https://www.gsea-msigdb.org/gsea/downloads.jsp/ [27,28].

2.13. Statistical analysis

One-way ANOVA with post hoc Tukey or multiple comparison analysis was used to determine the significant differences between 3 or more groups, and a t-test (equal variance, 2-tailed) was used to determine the significant difference between 2 groups. $P \leq 0.05$ was considered significant.

3. RESULTS

3.1. β-oxidation enzymes are localized to both mitochondria and nuclei and influence histone acylation

Using mass spectrometry, we previously revealed that all fatty acid β-oxidation enzymes reside in the nucleus in association with H2A.Z-bound chromatin [4]. ACAA2 is the enzyme that catalyzes the last step of the β-oxidation spiral, converting acetoacetyl-CoA into 2 acetyl-CoA molecules. To validate its nuclear presence and determine the effect of diet on its chromatin association, we performed an anti-ACAA2 ChIP—Seq assay on chromatin extracted from the heart tissue of mice fed either a low- (10 Kcal %) or high-fat (60 kcal %) diet for 4 days before subjecting them to a sham or transverse aortic constriction (TAC) surgery for one week while being sustained on the same diets. The TAC surgery imposed stress on the heart in the form of pressure overload, which induced hypertrophy of the cardiac myocytes associated with transcriptional remodeling. Within one-week post-TAC, there was $\sim$25% increase in heart mass, with no signs of cardiac dysfunction (Supplementary Figure 1S). Notably, the high-fat diet did not increase body weight within this period (Supplementary Figure 1S).

ACAA2 ChIP—Seq collective reads were plotted as average signals (Figure 1A—B) or shown in heatmaps across the TSS region ($-$2 Kb to $+$2 Kb) (Figure 1C—D). The numbers of total filtered peaks in the different conditions were as follows: 2,244 in Sham (10% fat), 1,843 in TAC (10% fat), 607 in Sham (60% fat), and 1,415 in TAC (60% fat) hearts. The number of peaks relative to genomic annotations are displayed in Supplementary Figure 2S. The fraction of reads in peaks (%, FRiP) was as follows: 0.7% in Sham (10% fat), 0.54% in TAC (10% fat), 0.15% in Sham (60% fat), and 0.39% in TAC (60% fat). The FRiP values were below the 1% threshold described by ENCODE; however, this was acceptable in cases where the protein has few binding sites, as seen with ZNF274 and human RNA polymerase III [29]. The results showed that TAC-induced stress reduced total peaks in the presence of a low-fat diet, whereas it increased it with a high-fat diet. This was also reflected in the representative gene promoters (*Clasp1*, *Arpc4*, and *Usp1*), where the ACAA2-bound sequence fragments aligned with the chromosome coordinates (Figure 1E). With no DNA-binding domain, we deduced that the association of ACAA2 with chromatin was expected to be indirect, which may have influenced the robustness of the ChIP—Seq data.

To determine whether β-oxidation contributes to histone butyrylation, we examined the abundance of H3K9Bu in human Hap1 cells with or without a deletion in the ACAA2 (ΔACAA2), hydroxyacyl-CoA dehydrogenase (ΔHADHA), or ACADS (ΔACADS) genes. The deletion of ACAA2 was expected to reduce the overall rate of β-oxidation, as acetoacetyl-CoA accumulation inhibits the enoyl-CoA hydratase long-chain enzyme (trifunctional enzyme) [30], similar to the deletion of

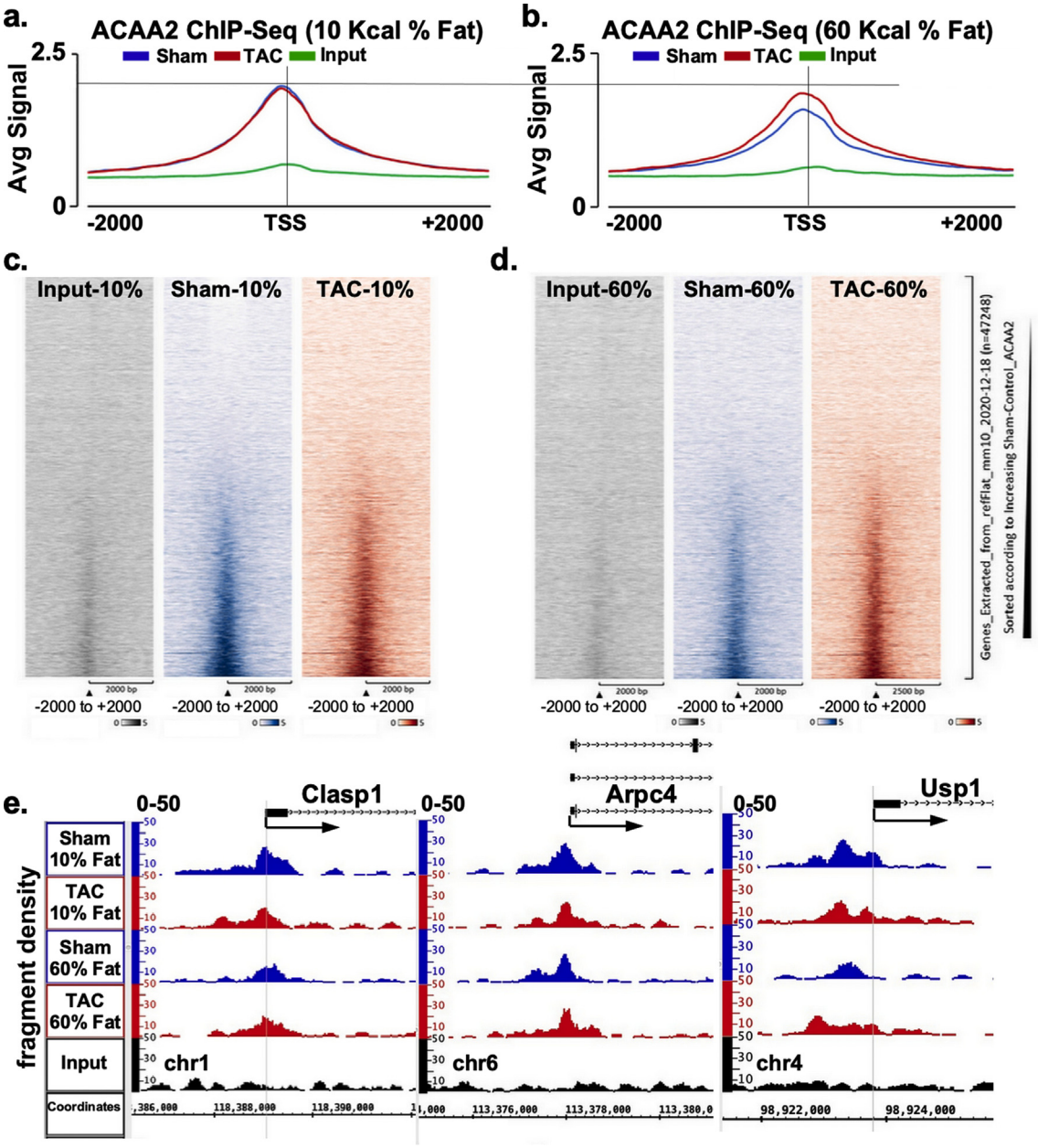

Figure 1: ACAA2 is associated with promoters and required for H3K9 butyrylation. Twelve-week-old C57BL/6J mice were maintained on a low-fat (10 Kcal %) or high-fat (60 Kcal %) diet for 4 days before subjecting them to transverse aortic constriction (TAC) or sham surgeries. They were then maintained on the same diets for 7 days before they were assessed by echocardiography, sacrificed, and the hearts isolated and pooled (n = 3 each). Chromatin was extracted from the heart tissue and subjected to anti-ACAA2 ChIP—Seq. **A—B.** The average signal (Avg Signal) of the chromatin-bound ACAA2 sequence reads (Y axis) assembled at gene promotors (−2 Kb to +2 Kb from the transcription start sites [TSS], X axis) were graphed for each condition (see color keycode at top) or **C—D.** all reads were represented by heatmaps aligned across the same region. Each input was generated from a pool of Sham and TAC heart chromatin. **E.** ACAA2-bound sequence fragments (Y axis) aligned to chromosome coordinates (X axis) are shown for *Clasp1*, *Arpc4*, and *Usp1* genes. Each ChIP—Seq reaction was conducted with a pool of 3 hearts (LV). The anti-ACAA2 ChIP—Seq was 2x for the low-fat diet with similar results (1 set, sham and TAC, in this figure and 1 set previously published, GEO accession # GSE119391) and 1x for the high-fat diet. **F.** A diagram of the β-oxidation pathway and the enzymes that catalyze it depicted in red. Deletion of ACADS (ΔACADS), HADHA (ΔHADHA), or ACAA2 (ΔACAA2) and its consequences on the intermediate metabolites are shown, where the upward arrow signifies an increase and the downward arrow signifies a decrease in the indicated intermediates. Accumulation of acetoacetyl-CoA upon deletion of ACAA2 inhibited the trifunctional enzyme activity. Short-chain acyl-CoA was salvaged by ketogenesis as depicted in light blue. **G.** Recombinant H3K9Ac, H3K9Bu, and H3K18Bu nucleosomes (25, 50, and 75 ng of protein) were analyzed by Western blotting using the corresponding antibodies. **H.** Protein from human Hap1, Hap1ΔACAA2, **J.** Hap1ΔHADHA, or **L.** ΔHap1ΔACADS cells was extracted, fractionated into cytosol (Cyto), membrane/mitochondria (Mem/mito), nucleoplasm (Nuc), and analyzed by Western blotting for the molecules listed on the right of each panel (n = 3—6 each). **I., K.,** and **M.** H3K9Bu or H3K9Cr signals were normalized to H3 or POL II, averaged, and the relative values calculated and graphed after adjusting one of the Hap1 sample levels to 1. Error bars represent S.E.M. The brackets encompass the values that were statistically compared for significance, with the p values listed above each.

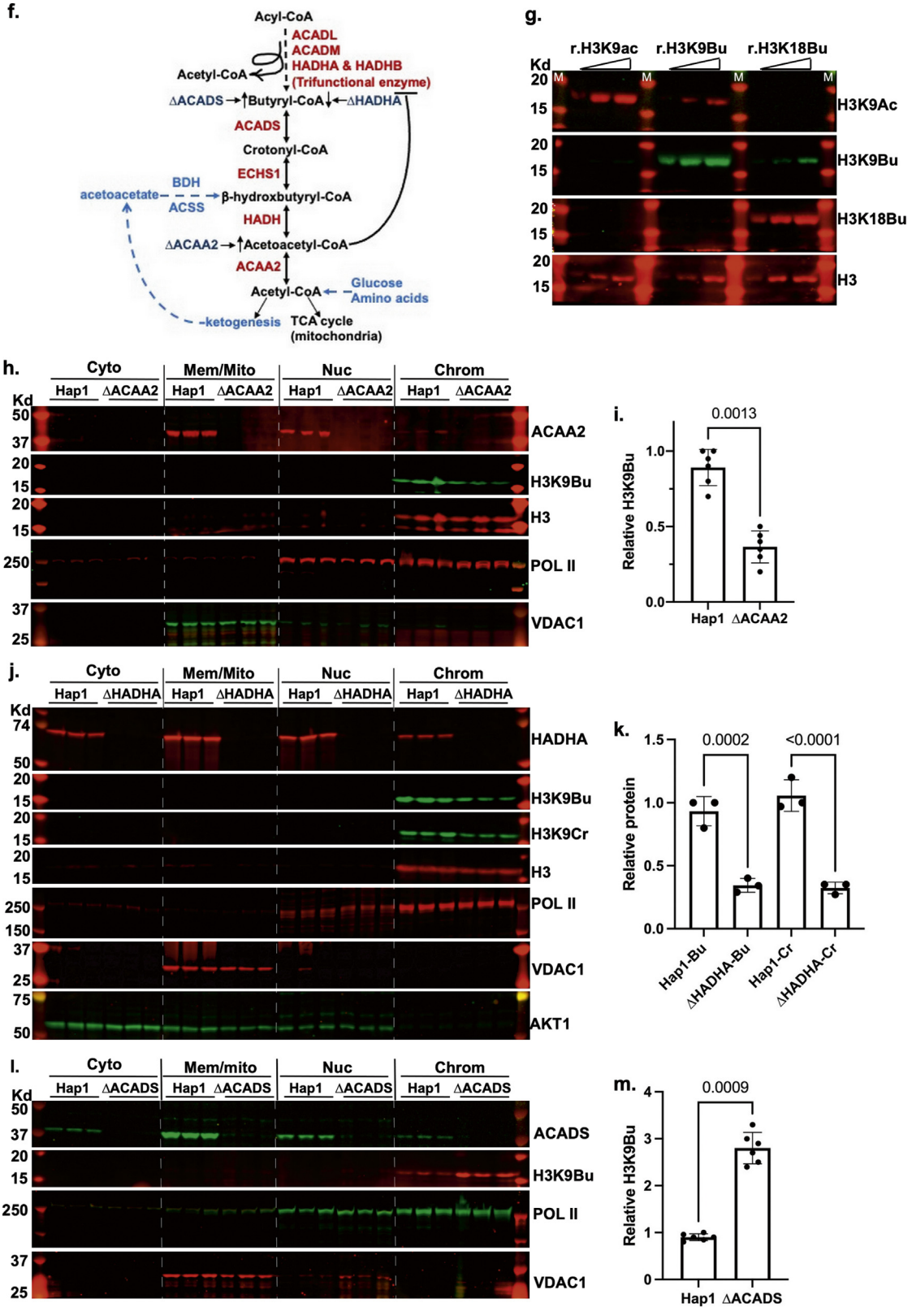

Figure 1: (*continued*).

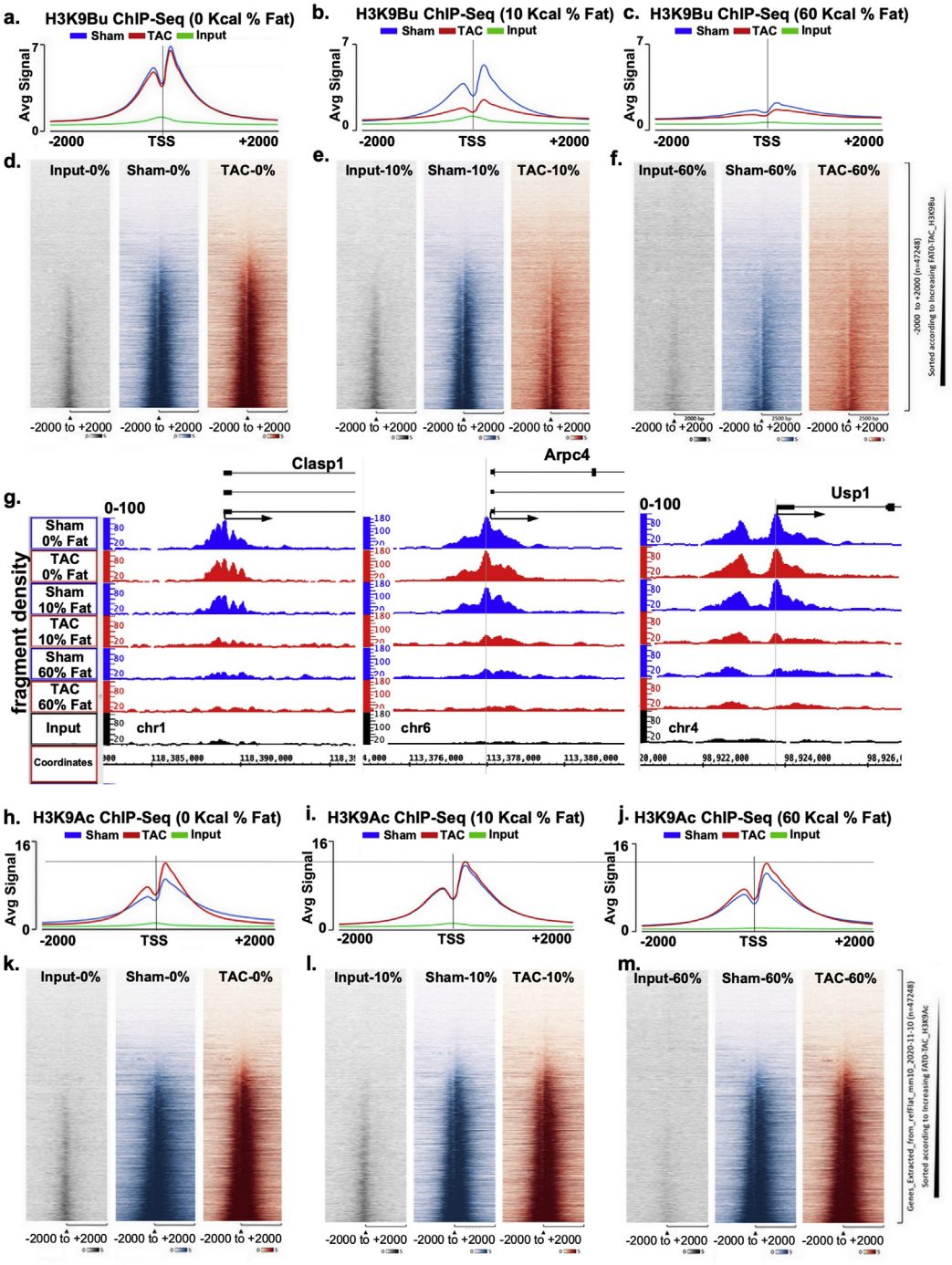

Figure 2: H3K9Bu encompasses TSSs and is modulated by dietary fat and stress. Twelve-week-old C57BL/6J mice were maintained on **A., D., H.,** and **K.** a fat-free (0 Kcal %), **B., E., I.,** and **L.** low-fat (10 Kcal %), or **C., F., J.,** and **M.** high-fat (60 Kcal %) diet for 4 days before subjecting them to transverse aortic constriction (TAC) or sham surgeries. They were then maintained on the same diets for 7 days before they were assessed by echocardiography, sacrificed, and the hearts isolated and pooled (n = 3 each). Chromatin was extracted from the heart tissue and subjected to **A**–**G.** anti-H3K9Bu or **H**–**M.** anti-H3K9Ac ChIP–Seq (n = 1, pool of 3 hearts each). **A**–**C** and **H**–**J.** Curves representing the average signal (Avg Signal) of the chromatin-bound sequence reads assembled at all the gene promoters (−2 kb to +2 kb from the TSS, see color keycode at top). Each input was generated from a pool of Sham and TAC heart chromatin. **D**–**F.** and **K**–**M.** Heatmaps representing the sequence reads aligned across the same region. **g.** H3K9Bu-bound sequence fragments aligned (Y axis) to chromosome coordinates (X axis) are shown for *Clasp1*, *Arpc4*, and *Usp1* genes.

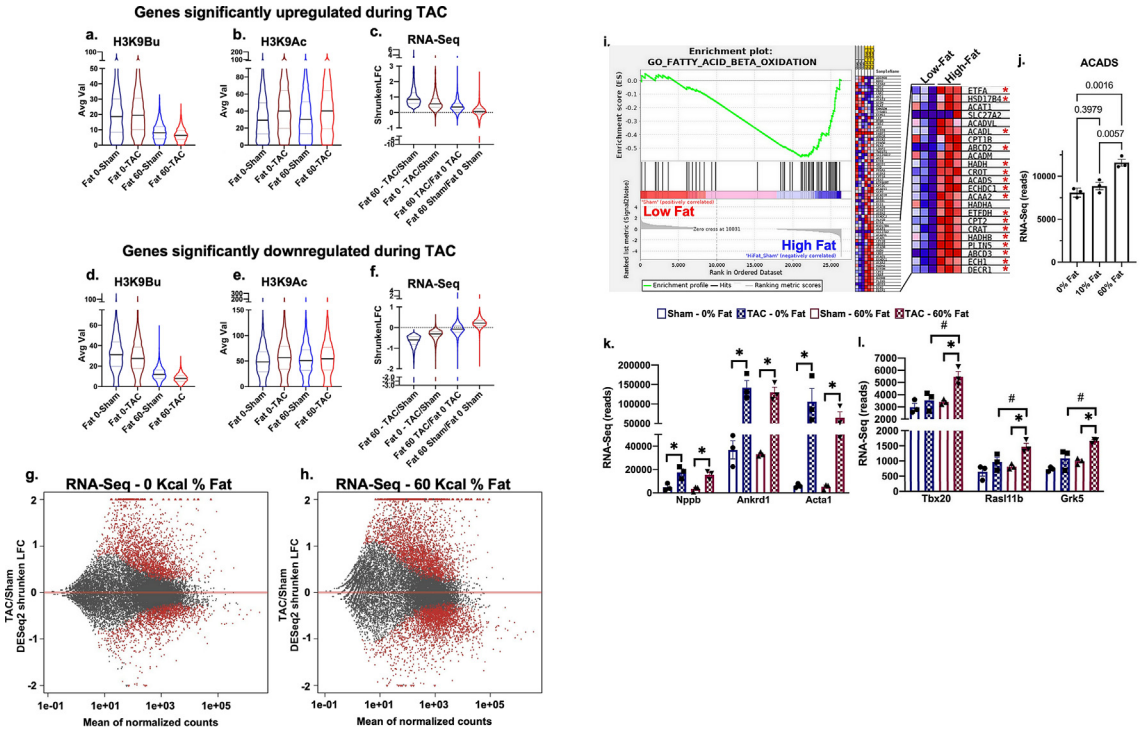

Figure 3: Higher levels of H3K9Bu correlate with blunted stress- and diet-induced changes in gene expression. Twelve-week-old C57BL/6J mice were fed a fat-free (0 Kcal % fat) or high-fat (60 kcal % fat) diet for 4 days before subjecting them to transverse aortic constriction (TAC) or sham surgeries. They were then maintained on the same diets for 7 days before they were assessed by echocardiography, sacrificed, and the hearts isolated and pooled for ChIP—Seq assay with anti-H3K9Bu or anti-H3K9Ac (n = 1, pool of 3 hearts each) or the RNA was extracted for RNA-Seq (n = 3 independent hearts each). **A**—**F.** The results were sorted according to mRNA of genes that were significantly ($p \leq 0.05$) **A**—**C.** upregulated (2,221 genes) or **D**—**F.** downregulated (2,242 genes) during TAC and a 60 kcal % fat diet (Fat 60 diet). **a.** and **d.** Violin plots showing the median and quartiles of H3K9Bu and **B.** and **E.** H3K9Ac average values of reads at the promoter regions (−1 kb to +1 kb) after subtracting the input for each. **c.** and **F.** Violin plots of the median and quartiles of the shrunken $\log_2$ fold change (LFC) of the RNA-Seq for fat-free (Fat 0) TAC/Sham, Fat 60 TAC/Sham, Fat 60 TAC/Fat 0 TAC, and Fat 60 Sham/Fat 0 Sham. **G.** and **H.** MA plots of the DeSeq2 shrunken LFC (Y axis) vs mean of normalized counts (X axis) of the TAC/Sham RNA-Seq data with the different diets. **I.** A gene enrichment plot of GO term fatty acid β-oxidation generated from the heart tissue RNA-Seq data (n = 3) from the mice maintained on the low-fat (10% fat) vs high-fat (60% fat) diet for 11 days. Heatmap of the differentially expressed genes is shown on the right. The red asterisks indicate $p < 0.05$. **J.** RNA-Seq reads for ACADS mRNA from the heart tissue of the mice on the indicated diets were averaged and plotted. Error bars represent S.E.M. The brackets encompass the values that were statistically compared for significance, with the p values listed above each. **K**—**L.** RNA-Seq results for **K.** Nppb, Ankrd1, and Acta1, or **L.** Tbx20, Rasl11b, and Grk5 were averaged (n = 3) and plotted as bar graphs (see color keycode at top). * indicates $p \leq 0.05$ vs Sham and # indicates $p \leq 0.05$ vs TAC. **M**—**N.** H3K9Bu- and H3K9Ac-bound sequence fragments (Y axis) aligned to the chromosome coordinates (X axis) are shown for the genes in (**K**—**L.**). **O.** Gene enrichment plots of GO term respirasome generated from the Sham vs TAC heart tissue RNA-Seq data (n = 3, each) from the mice maintained on a 0, 10, or 60 kcal % fat diets, with a heatmap of the differentially expressed genes shown on the right of each.

HADHA, and in turn will reduce the abundance of acyl-CoA intermediates (Figure 1F). In contrast, the deletion of ACADS was expected to increase butyryl-CoA and therefor histone butyrylation (Figure 1F). Protein from the Hap1, Hap1 ΔACAA2, ΔHADHA, or ΔACADS cells was extracted, fractionated, and analyzed by Western blotting. The results confirmed the localization of the ACAA2, HADHA, and ACADS proteins to both mitochondria and nuclei, which were eliminated from the corresponding knockout cells. To determine how these knockouts impact H3K9Bu, we first confirmed the specificity and efficiency of anti-H3K9Bu using modified recombinant H3K9Ac, H3K9Bu, and H3K18Bu protein, the results of which revealed little or no detectable, nonspecific, cross-reactivity of the specific antibodies (Figure 1G). We also showed that anti-H3K9Bu antibody did not detect H3K9-crotonyl or H3K9-b-hydroxybutyryl (Supplementary Figure. 3S). The data showed that the deletion of either ACAA2 or HADHA reduced the abundance of H3K9Bu and H3K9Cr (Figure 1H—K), whereas ΔACADS significantly increased H3K9Bu (Figure 1L—M) in accordance with expectations if histone butyrylation was a product of β-oxidation (Figure 1F). Antibodies against histone H3, Pol II, VDAC1, and AKT1 were used as internal controls and to distinguish the protein fractions. We predict that H3K9 butyrylation is a product of β-oxidation in the nucleus, where we detect the catalyzing enzymes. However, we cannot exclude the posiibility that butyryl-CoA is also exported from the mitochondria [12].

3.2. H3K9Bu is enriched at transcription start sites and downregulated by dietary fat and stress

If histone butyrylation is a product of β-oxidation, then it is likely to be modulated by dietary fat. Therefore, to examine the effect of dietary fat on H3K9Bu abundance and genomic distribution in the healthy or stressed heart, we performed ChIP—Seq analysis with chromatin extracted from heart tissue of mice fed either a fat-free (0 kcal %), low-fat (10 kcal %), or high-fat (60 kcal %) diet for 4 days. The mice were then subjected to either a sham or TAC surgery followed by a one-week survival period while they were sustained on the same diets. Body weight and cardiac functions were normal within this period (Supplementary Figure 1S). There was no difference between the extent of hypertrophy with the different diets (see also Figure 3K).

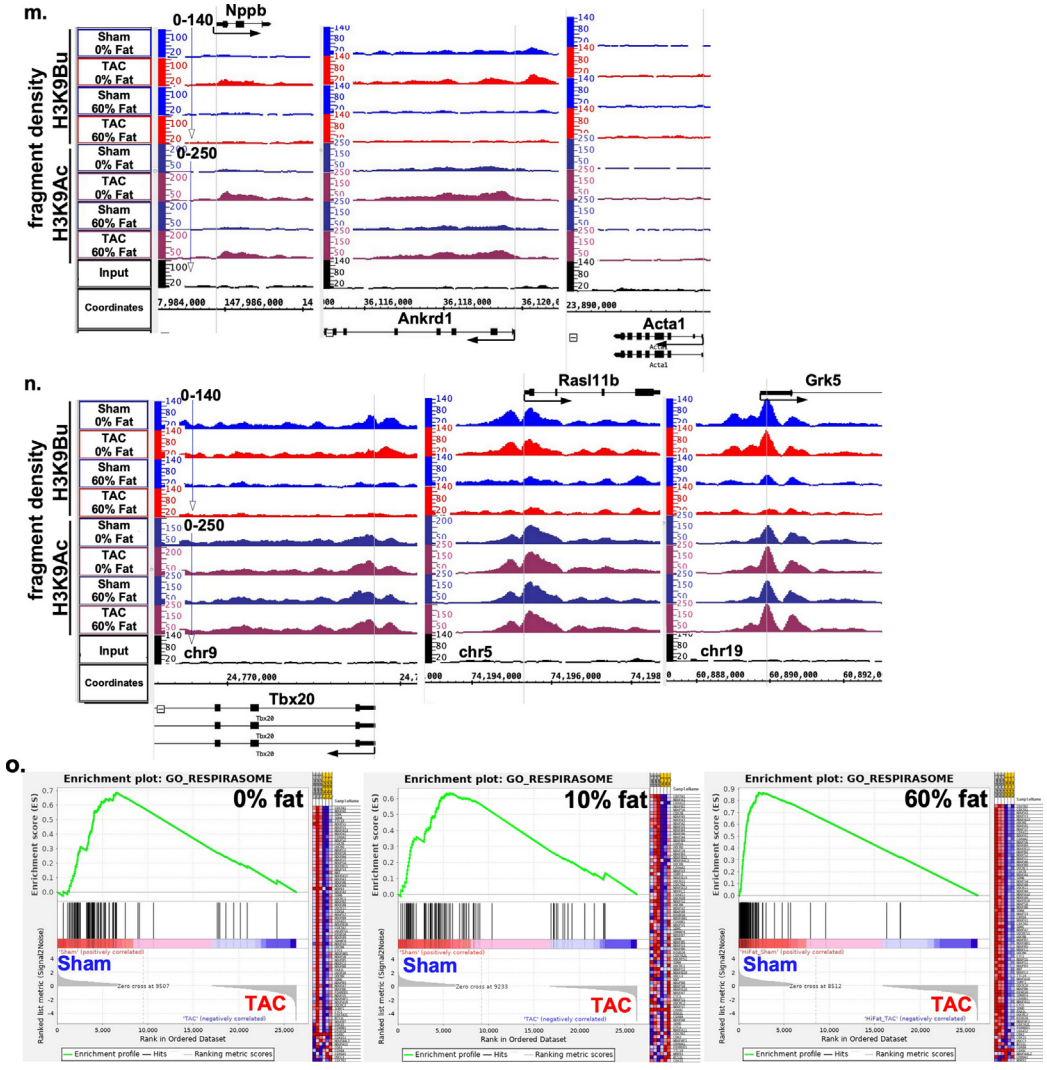

Figure 3: (*continued*).

H3K9Bu ChIP—Seq reads were plotted as average signals or shown in heatmaps across the TSS region (−2 kb to +2 kb). The results showed the enrichment of H3K9Bu surrounding the TSSs (Figure 2A—F). The numbers of total filtered peaks with the different conditions were as follows: 40,287 in Sham (0% fat), 35,349 in TAC (0% fat), 41,838 in Sham (10% fat), 24,082 in TAC (10% fat), 33,947 in Sham (60% fat), and 16,768 in TAC (60% fat). The numbers of peaks relative to genomic annotations are displayed in Supplementary Figure 2S. FRiP (%) values was as follows: 22.53% in Sham (0% fat), 18.26% in TAC (0% fat), 17.06% in Sham (10% fat), 5.14% in TAC (10% fat), 7.24% in Sham (60% fat), and 2.95% in TAC (60% fat); these numbers are tabulated in Supplementary Table 1S. As predicted, the levels of H3K9Bu were indeed influenced by diet; however, counter to our prediction, the levels were reduced with increasing levels of dietary fat (Figure 2A—F) and surprisingly were highest in the hearts of the mice on a fat-free diet (Figure 2A,D). These effects were global as could be seen at the promoters of representative genes (*Clasp1*, *Arpc4*, and *Usp1*), where the sequence fragments were aligned with the chromosome coordinates (Figure 2G). This is also evident across the coordinates of whole chromosomes (Supplementary Figures 4S—a). Moreover, the levels were reduced by TAC-induced stress, which was more pronounced with the low- and high-fat diets vs. the fat-free diet. The data were confirmed by ChIP-qPCR (Supplementary Figures 5S—c). Thus, these results were the first demonstration of the genome-wide distribution of H3K9Bu in addition to its differential regulation by diet and stress. The causes of the reduction in H3K9Bu with the high-fat vs fat-free or low-fat diets and the source of butyryl-CoA associated with the fat-free diet are shown in Figures 3 and 4.

We next addressed how diet-induced changes in H3K9Bu correlate with H3K9Ac abundance in the normal and stressed heart. For that purpose, we conducted an anti-H3K9Ac ChIP—Seq assay from the same chromatin used for H3K9Bu ChIP—Seq. H3K9Ac ChIP—Seq reads were plotted as average signals or shown in heatmaps across the TSS region (−2 Kb to +2 Kb). The results showed the enrichment of H3K9Ac surrounding the TSSs (Figure 2H—M). The numbers of total filtered peaks with the different conditions were as follows: 30,778 in Sham (0% fat), 26,577 in TAC (0% fat), 31,850 in Sham (10% fat), 30,855 in TAC (10% fat), 32,366 in Sham (60%

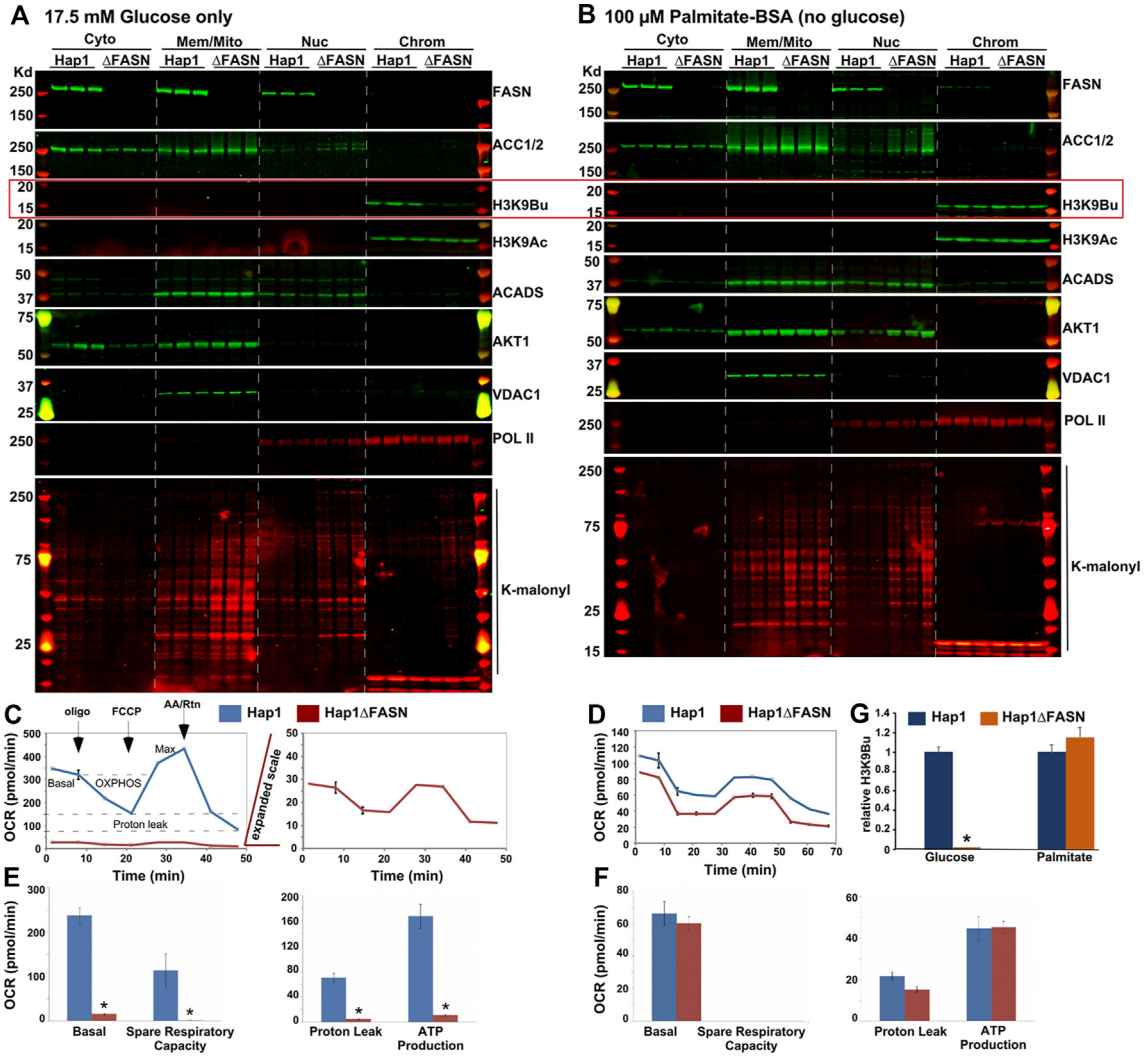

Figure 4: FASN is required for H3K9 butyrylation in the absence of fatty acids. A—B. Hap1 and Hap1ΔFASN cells were cultured to near confluency before the fetal bovine serum was removed and the cells were maintained in **A., C.,** and **E.** DMEM with 17.5 mM of glucose or **B., D.,** and **F.** DMEM (no glucose) with 100 µM of palmitate-BSA. **A—B.** After ~20 h, the protein was extracted, fractionated, and analyzed by Western blotting as described in A. **C—F.** Cells maintained in **C.** and **E.** glucose only or **D.** and **F.** palmitate only were subjected to a Mito Stress Test using an extracellular flux analyzer (XF^{e}96). Oxygen consumption rates (OCR) were measured in live cells before and after sequentially treating the cells with oligomycin (oligo), FCCP, and anti-mycin A and rotenone (AA/Rtn) as indicated by the arrows shown on the curve in **E. C—D.** The curves represent the real-time measurements of the OCR (*p*mole/min, Y axis) vs time (min, X axis). **E—F.** The bar graphs represent the mitochondrial basal OCR (last rate measured before oligo injection minus non-mitochondrial respiration rate), SRC (the difference maximum [which was the maximum measurement after FCCP injection minus the non-mitochondrial respiration rate] and basal respiration), proton leak (minimum rate measured after oligo injection minus non-mitochondrial respiration), and ATP production levels (last rate measured before oligo injection minus the minimum rate after oligo injection). **G.** Western blotting signals for H3K9Bu in **A.** and **B.** were quantitated, normalized to H3K9Ac, averaged, and graphed. Error bars represent S.E.M. and $p \leq 0.05$ vs Hap1.

fat), and 31,873 in TAC (60% TAC). The numbers of peaks relative to genomic annotations are displayed in Supplementary Figure 2S. Although the total numbers of peaks were slightly reduced by TAC with all 3 diets, FRiP (%) increased incrementally, 31.46% in Sham (0% fat), 32.15% in TAC (0% TAC), 32.44 in Sham (10% fat), 32.82 in TAC (10% fat), 31.56% in Sham (60% fat), and 34.62% in TAC (60% fat), which was reflected in the promoter peaks (Figure 2H—J); these numbers are tabulated in Supplementary Table 1S. Thus, in contrast to promoter-H3K9Bu, cumulative promoter-H3K9Ac did not exhibit substantial changes in the unstressed hearts with the different diets, increasing incrementally after stress (Figure 2H—M). This is also evident across the coordinates of whole chromosomes (Supplementary Figure 4S).

3.3. Higher levels of H3K9Bu coincide with blunted stress- and diet-induced changes in gene expression

To study the relationship between diet, H3K9Bu, H3K9Ac, and gene expression, we performed RNA-Seq using the same conditions. We then integrated the results of the ChIP—Seq (promoter regions) and RNA-Seq. The genes were then sorted according to those that were either significantly ($p \leq 0.05$) upregulated or downregulated in the hearts of the high-fat-fed mice post-TAC. The results were graphed as violin plots of the medians and quartiles (Figure 3A—F). The means of the same data sets were calculated, graphed, and analyzed, revealing significant differences between all of the compared conditions (Supplementary Figure 5Sa—b). These results confirmed the global nature of the changes in promoter-H3K9Bu with

diet, where it was highest with fat-free vs high-fat diet and reduced slightly after TAC (Figure 3A,D). In contrast, H3K9Ac increased (~25%) post-TAC at the promoters of genes whose expression was upregulated (Figure 3A). However, H3K9Ac was not collectively reduced at the promoters of downregulated genes but was selectively reduced. H3K9Ac at the promoters of constitutively expressed housekeeping genes increased incrementally (Supplementary Figure 6S) in parallel with the reported incremental RNA polymerase II pause release at their promoters, which underlies cardiac hypertrophy [31]. The RNA-Seq data revealed that TAC induced both overall greater increases and decreases in gene expression in the hearts of the high-fat- vs fat-free-fed mice (Figure 3C,F). This was also displayed in the MA plots, where the red dots representing all RNA-Seq data points with p values < 0.1 showed a wider range of both positive and negative LFC with the high- vs low-fat diet (Figure 3G—H). The figure also reveals a higher number of genes dysregulated by stress during the high-fat vs fat-free fat diet. With the high-fat diet, there were 2,221 genes upregulated and 2,242 downregulated significantly, $p \leq 0.5$; with the fat-free diet, there were 1,589 genes upregulated and 1,074 genes downregulated significantly, $p \leq 0.5$. Diet also induced significant changes in basal gene expression, albeit subtle (Supplementary Figure 6S). The high-fat vs low-fat diet significantly increased the basal expression of β-oxidation genes as demonstrated in the gene enrichment plot, GO fatty acid β-oxidation (Figure 3I). The heatmap on the right reveals that some of these genes, which included ACADS, exhibited a significant increase vs low-fat diet levels (Figure 3J). This finding may explain the reduced levels of H3K9Bu after the high-fat diet, as the increase in ACADS was expected to accelerate the reduction of butyryl-CoA to crotonyl-CoA. On the other hand, β-oxidation enzymes are downregulated in the heart post-TAC, which may be the reason for further reductions in H3K9Bu.

At this time point (1 week post-TAC), TAC-induced increase in the left ventricular (LV) mass was similar in the mice on the low- or high-fat diet (Supplementary Figure 1S). We also confirmed that some of the established cardiac hypertrophy markers, including Nppb, Ankrd1, and Acta1, equally increased with both diets (Figure 3K). This confirmed that the overall differences observed in gene expression with the different diets (Figure 3G—H) were not due to variations in the extent of TAC-imposed stress on the heart. In contrast to the cardiac hypertrophy markers, other genes exhibited significantly higher increases (1.5- to 2-fold) in the high-fat-fed mice (Tbx20, Rasl11b, and Crk5, Figure 3L). Notably, genes such as Nppb, Ankrd1, and Acta1 that were insensitive to the type of diet exhibited a relatively more robust increase in expression post-TAC (3—100-fold) and had significantly less promoter-H3K9Bu (Figure 3M) vs the latter group (Figure 3N). In contrast, H3K9Ac in both gene groups increased similarly post-TAC with both diets, suggesting that the differences in gene expression with the different diets were not due to differences in promoter-H3K9Ac.

As with the upregulated genes, the high-fat diet also amplified TAC-induced decreases in gene expression. Gene Set Enrichment Analysis (GSEA) revealed GO respirasome as one of the most significant diet-dependent differential gene expression in the heart (Figure 3O). The GSEA plots and corresponding heatmaps (right) uncovered a more pronounced downregulation of mitochondrial respiratory genes in the TAC-stressed hearts of the mice on the high-fat vs low-fat or fat-free diet, but none in the unstressed sham hearts. Thus, while levels of promoter H3K9Ac did not vary much with the diet, lower H3K9Bu induced by the high-fat diet and stress coincided with exaggerated changes in gene expression, implicating it in worse disease outcomes.

3.4. In the absence of fatty acids, fatty acid synthesis from glucose reconstitutes H3K9 butyrylation

We predicted that histone butyrylation is a product of butyryl-CoA produced by β-oxidation. However, the results shown in Figure 2 contradict this hypothesis, as the mice fed the fat-free diet had the highest levels of H3K9Bu. One possibility was that fatty acids synthesized from carbohydrate were the source of butyryl-CoA necessary for histone butyrylation. Fatty acid synthase (FASN) is an enzyme that catalyzes the synthesis of long-chain fatty acids from citrate that is exported from the mitochondria during nutrient abundance after it is sequentially converted into malonyl-CoA by ATP citrate lyase and carboxylase 1 and 2 (ACC1/2) [32]. First we confirmed that (FASN) and (ACC1/2) were expressed in the mouse heart, where we also showed that they increased significantly after TAC (Supplementary Figure 8Sa—b). To determine the role of FASN in H3K9 butyrylation, we used human Hap1 cells with or without a deletion in the *FASN* gene (Hap1ΔFASN). The knockout cells were healthy and proliferated at near normal rates; however, they were smaller in size relative to the parent cells (Supplementary Figure 8Sc—d). The cells were cultured in medium containing either glucose or palmitate only for ~20 h before the protein was extracted and analyzed by Western blotting. As expected, the ΔFASN cells were devoid of FASN protein and exhibited greater levels of lysine-malonyl as its substrate, malonyl-CoA, accumulated in these cells (Figure 4A—B). When they were maintained in a high-glucose fatty acid-free medium, the ΔFASN cells had <5% of H3K9Bu vs the parent Hap1 cells, while H3K9Ac levels were unaffected (Figure 4A,G). In contrast, when the knockout cells were maintained in medium with palmitate-BSA, they had slightly higher levels of H3K9Bu vs the parent cells (Figure 4B,G).

We also questioned whether the FASN-synthesized fatty acids were stored or utilized by the cells, considering that glucose was in abundance. To address this, we used the same culturing conditions previously described to measure the oxygen consumption rates (OCR) in these cells. The working hypothesis was that if the FASN-synthesized fatty acid was being oxidized for fuel even in the presence of glucose, then deletion of FASN would reduce the OCR. Notably, the results showed that the OCR was reduced by ~90% in the ΔFASN cells, including the basal capacity, spare respiratory capacity, proton leak, and ATP-linked OCR (Figure 4C,E). This indicated that even in the presence of high glucose, these cells predominantly utilized FASN-synthesized fatty acids for energy. In comparison, the ΔFASN cells cultured with palmitate-BSA showed no significant differences in the OCR relative to the parent cells (Figure 4D,F). These results are evidence that H3K9 butyrylation requires β-oxidation, where in the absence of fatty acid substrate, fatty acid synthesized from glucose-derived acetyl-CoA is the substitute.

3.5. ACADS localizes to both mitochondria and nuclei and its deletion increases H3K9Bu in the mouse heart

ACADS is recognized as a mitochondrial protein involved in the β-oxidation spiral, where it reduces butyryl-CoA to crotonyl-CoA (Figure 1F). The Human Protein Atlas documented its nuclear localization as well [33]. The Western blotting shown in Figure 1J confirmed its nuclear presence in human Hap1 cells. For further confirmation, we fused its C-terminus to turbo-green fluorescence protein (tGFP) and delivered the construct to cultured cardiac myocytes. Western blotting analysis of the protein showed that tGFP localized to the cytosol and membrane/mitochondrial fractions, with none detected in the nuclear fraction (Figure 5A—B). However, when it fused to ACADS, the protein redistributed to the membrane/mitochondrial and nuclear fractions (Figure 5A and 5B, top panel). This localization overlapped with the

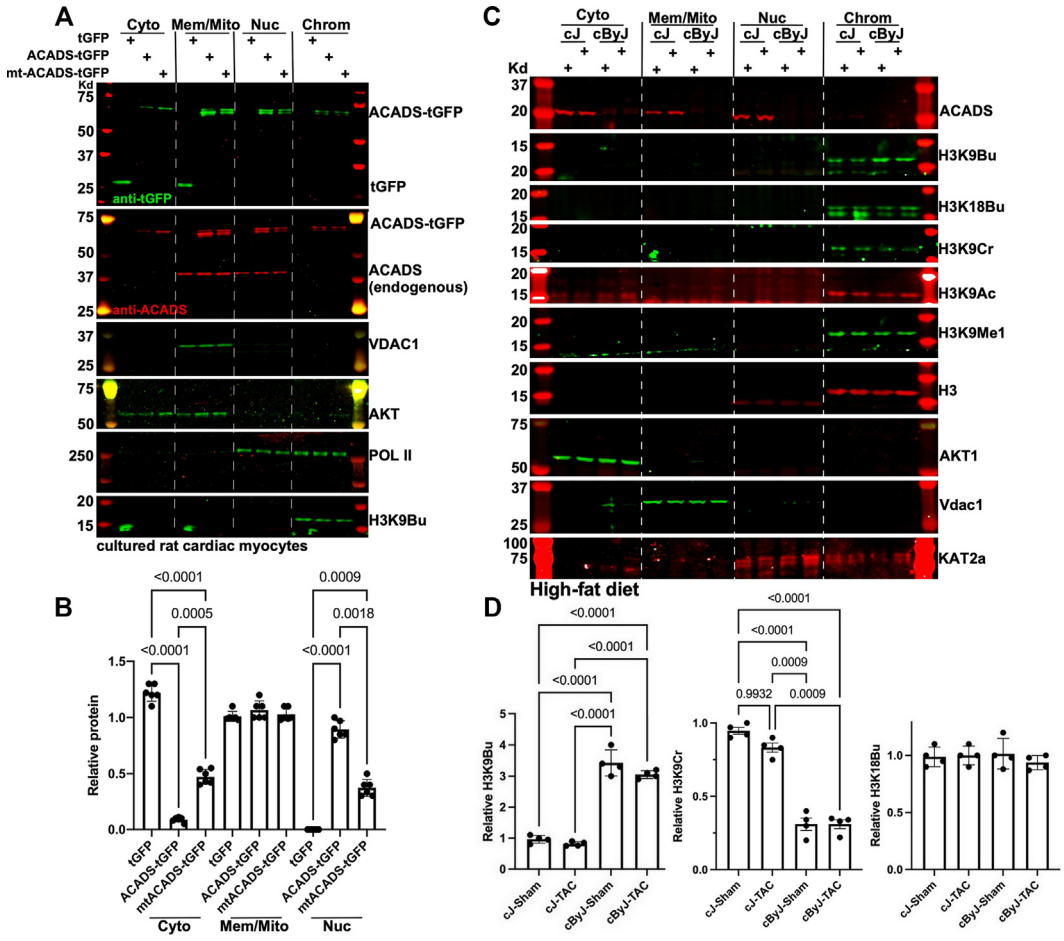

Figure 5: ACADS is a mitochondrial and nuclear protein and its deficiency is associated with a specific increase in H3K9Bu. A—B. Cardiac myocytes were isolated and cultured for 24 h before they were supplemented with Ad-tGFP, Ad-ACADS-tGFP, or Ad-NLS-mutant ACADS (Ad-mt-ACADS) for an additional 24 h before the cells were harvested. **C—D.** Twelve-week-old Balc/cJ and Balb/cByJ (ACADS-deficient) mice were maintained on a high-fat (60 Kcal %) diet for 4 days before subjecting them to transverse aortic constriction (TAC) or sham surgeries. They were then maintained on the same diet for 7 days before they were assessed by echocardiography, sacrificed, and the hearts isolated. **A.** and **C.** Protein from isolated cardiac myocytes or heart tissue was fractionated into cytosol (Cyto) membranes, including mitochondria (Mem/Mito), nucleoplasm (Nuc), and chromatin (Chrom). The protein was analyzed by Western blotting with antibodies for the molecules listed on the right of the panels or **A.** with anti-tGFP (top panel) or anti-ACADS (second from the top panel). The first and last lanes show protein standards, and their sizes are listed on the left of each panel. **B.** and **D**. Western blotting signals were quantitated, and cytosolic proteins were normalized to AKT1, membrane/mitochondrial protein to VDAC1, nucleoplasm proteins to Pol II, and H3K9Bu to H3 or Pol II ($n = 4—6$ each). **D**. The results were plotted relative to a cJ-Sham signal adjusted to 1. **B.** Signals for tGFP, ACADS-tGFP, and mt-ACADS-tGFP in the Cyto and Nuc fractions were plotted each relative to its corresponding Mem/Mito signal adjusted to 1. Error bars represent S.E.M. The brackets encompass the values that were statistically compared for significance, with the p values listed above each.

endogenous ACADS (Figure 5A, second panel from the top). Moreover, when a mutation was introduced into a putative NLS sequence in that gene (Supplementary Figure 9S), it reduced its nuclear localization while increasing it in the cytosol.

Thus, we show that ACADS is a nuclear and mitochondrial protein and propose that it functions in steps in the β-oxidation pathway in the nucleus, regulating the accumulation of butyryl-CoA and in turn H3K9 butyrylation. The fact that knockout of ACADS in human Hap1 cells increased H3K9Bu supports this concept. We also tested this idea in Balb/cByJ (cByJ) mice, which were deficient in ACADS as a result of a spontaneous deletion mutation in the gene [34], and their wild-type Balb/cJ (cJ) counterparts. The mice were maintained on a 60 kcal % fat (or 10% kcal) (Supplementary Figure 10S) diet for 4 days before subjecting them to a sham or TAC surgery for 7 days. Protein from the heart tissue was extracted, fractionated, and analyzed by Western blotting. The results confirmed that the ACADS protein was absent in the cByJ-deficient mice and was associated with a more than 3-fold increase in H3K9Bu, with no significant reduction after TAC (Figure 5C—D). In contrast, levels of H3K9Cr were significantly reduced, suggesting that H3K9Cr is also a product of β-oxidation reactions in the nucleus and inversely regulated by ACADS. Intriguingly, levels of H3K18Bu remained unchanged (see validation of antibody specificity in Figure 1G), demonstrating the highly specific and regulated nature of histone modification.

3.6. Deletion of ACADS reverses stress-induced downregulation of H3K9Bu

H3K9Bu was not only reduced by the high-fat diet but also by pressure overload-induced stress (Figure 2B—C). We hypothesized that this reduction was mediated by enhanced ACADS activity. To test this, we performed H3K9Bu ChIP—Seq on the hearts of the Balb/cJ and ACADS-deficient Balb/cByJ mice one week after a sham or TAC surgery. H3K9Bu ChIP—Seq reads were plotted as average signals or shown in heatmaps across the TSS region (−2 Kb to +2 Kb). The

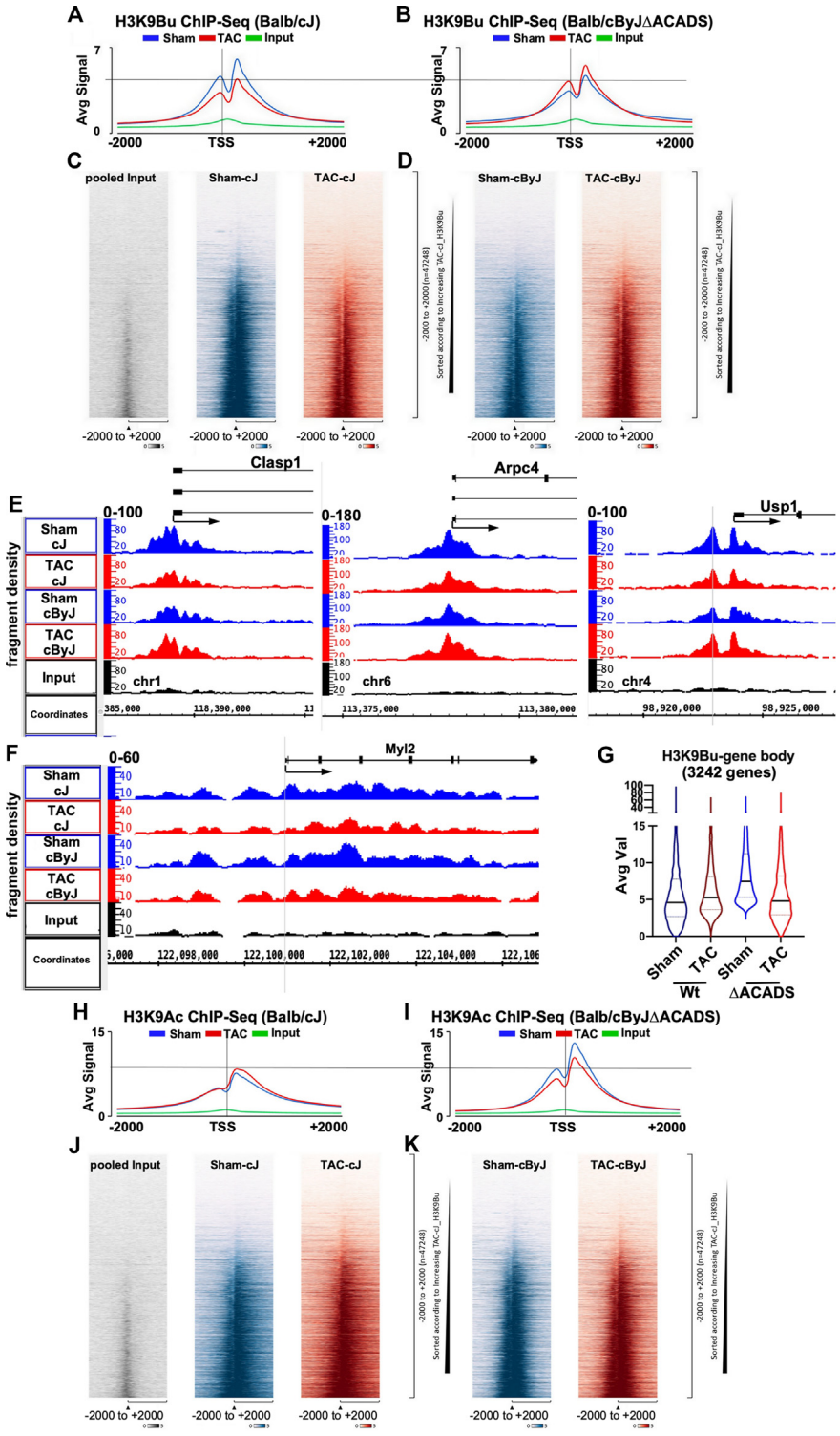

Figure 6: Deletion of ACADS reverses stress-induced downregulation of H3K9Bu in the heart. Twelve-week-old Balc/cJ and Balb/cByJ (ACADS-deficient) mice were maintained on a low-fat (10% of calories) diet for 4 days before subjecting them to transverse aortic constriction (TAC) or sham surgeries. They were then maintained on the same diet for 7 days before they were assessed by echocardiography, sacrificed, and the hearts isolated and pooled (n = 3, each). Chromatin was extracted from the heart tissue and subjected to anti-H3K9Bu ChIP–Seq (n = 1, a pool of 3 hearts each). **A–B.** The average signal (Avg Signal) of the chromatin-bound H3K9Bu reads assembled at all of the gene promotors (−2 Kb to +2 Kb from the TSS) were plotted for each condition (see color keycode at top) **C–D.** or all sequence reads were represented by a heatmap across the same region. **E–F.** H3K9Bu-bound sequence fragments (Y axis) aligned to chromosome coordinates (X axis) are shown for *Clasp1*, *Arpc4*,*Usp1*, and *Myl2* genes. **g.** Violin plots showing the median and quartiles of H3K9Bu average values of sequence reads within gene bodies in 3,242 genes (+1 Kb from TSS to gene end). **H–I.** The average signal (Avg Signal) of the chromatin-bound H3K9Ac reads assembled at all of the gene promotors (−2 Kb to +2 Kb from the TSS) graphed for each condition (see color keycode at top) or **J–I.** all reads were represented by heatmaps across the same region. The input was generated from a pool of Balb/cJ and Balb/cByJ, Sham, and TAC heart chromatin.

numbers of total filtered peaks with the different conditions were as follows: 44,416 in Sham (Balb/cJ), 28,975 in TAC (Balb/cJ), 38,596 in Sham (Balb/cByJ-ΔACADS), and 40,745 in TAC (Balb/cByJ-ΔACADS). FRiP values (%) were as follows: 20.42% in Sham (Balb/cJ), 10.69% in TAC (Balb/cJ), 15% in Sham (Balb/cByJ-ΔACADS), and 17.41% in TAC (Balb/cByJ-ΔACADS); these numbers are tabulated in Supplementary Table 1S. The results showed the enrichment of H3K9Bu surrounding the TSSs, where in contrast to the wild-type mice, the ACADS-deficient mice exhibited an increase vs a decrease in promoter-H3K9Bu post-TAC stress (Figure 6A—D). These effects were global as can be seen at the promoters of representative genes (Clasp1, Arpc4, and Usp1), where the sequence tags aligned with the chromosome coordinates (Figure 6E). The data were confirmed by ChIP-qPCR (Supplementary Figures 5S—c).

Of note, unstressed levels of promoter-H3K9Bu in the sham mice were unchanged or slightly higher than in the wild-type vs ACADS-deficient mice. This contrasts with the Western blotting in Figure 5C, which shows higher total H3K9Bu, which includes H3K9Bu across all the genomic regions. One possibility is that H3K9Bu within other regions of the genome compensated for this difference. We therefore examined the levels of H3K9Bu within gene bodies. We observed that H3K9Bu extended into the gene bodies of 3,242 genes, where the ACADS-deficient mice had higher levels in the unstressed vs wild-type heart (Figure 6F—G and Supplementary Figure 11S), plausibly explaining the higher levels detected by Western blotting. Thus, deletion of ACADS did not increase unstressed promoter-H3K9Bu, but it did reverse its downregulation seen during stress, with an increase above normal levels. However, ΔACADS increased H3K9Bu within the gene bodies.

We also measured changes in H3K9Ac to determine how it correlates with H3K9Bu. H3K9Ac ChIP—Seq was performed using the same chromatin used for H3K9Bu ChIP—Seq. The sequence reads were plotted as average signals or shown in heatmaps across the TSS region (−2 Kb to +2 Kb) (Figure 7A—D). The numbers of total filtered peaks with the different conditions were as follows: 34,545 in Sham (Balb/cJ), 36,934 in TAC (Balb/cJ), 32,117 in Sham (Balb/cByJ-ΔACADS), and 31,359 in TAC (Balb/cByJ-ΔACADS). FRiP values (%) were as follow: 27.87% in Sham (Balb/cJ), 31.46% in TAC (Balb/cJ), 37.42% Sham (Balb/cByJ-ΔACADS), and 29.75% in TAC (Balb/cByJ-ΔACADS). The results showed that in contrast to promoter-H3K9Bu, promoter-H3K9Ac was slightly upregulated by TAC in the wild-type mice, whereas unstressed levels were higher in the ACADS-deficient mice but downregulated post-TAC to levels nearing those in the wild-type mice (Figure 7H—K). Although unstressed levels of promoter-H3K9Ac were collectively higher in the ΔACADS mice, the total numbers of peaks were reduced but had a higher fraction of reads in peaks.

3.7. Deletion of ACADS blunts stress-induced changes in gene expression

With the fat-free vs high-fat diet, the heart exhibited much higher levels of H3K9Bu, which coincided with blunted stress-induced changes in

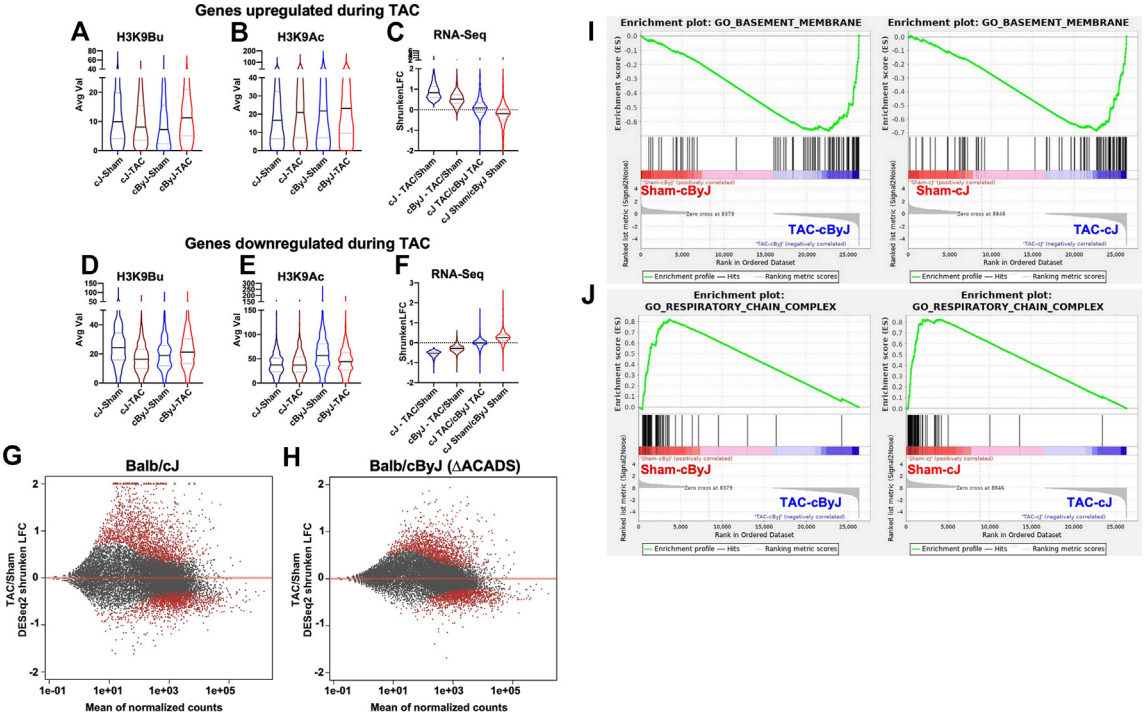

Figure 7: Deletion of ACADS blunts stress-induced changes in gene expression. Twelve-week-old Balc/cJ and Balb/cByJ (ACADS-deficient) mice were maintained on a low-fat (10% of calories) diet for 4 days before subjecting them to transverse aortic constriction (TAC) or sham surgeries. They were then maintained on the same diet for 7 days before they were assessed by echocardiography, sacrificed, and the hearts isolated and pooled (n = 3 each) for ChIP—Seq with anti-H3K9Bu or anti-H3K9Ac (n = 1, a pool of 3 hearts each) or the RNA was extracted for RNA-Seq (n = 3 independent hearts each). **A—F.** The results were sorted according to mRNA of genes that were significantly ($p \leq 0.05$) **A—C.** upregulated (1,272 genes) during TAC in the Balb/cJ mice (cJ) or **D—F.** downregulated (1,016) during TAC in the cJ mice. **A.** and **D.** Violin plots showing the median and quartiles of H3K9Bu and **B.** and **E.** H3K9Ac average values of sequence reads at the promoter regions (−1,000 to +1,000) after subtracting the input for each. **C.** and **F.** Violin plots of the median and quartiles of the shrunken $\log_2$ fold change (LFC) of the RNA-Seq for cJ-TAC/Sham, cByJ-TAC/Sham, cJ-TAC/cByJ-TAC, and cJ-Sham/cByJ-Sham. **G.** and **H.** MA plots of the DeSeq2 shrunken LFC (Y axis) vs mean of normalized counts (X axis) of the TAC/Sham RNA-Seq data for Balb/cJ and Balb/cByJ. **I—J.** Enrichment plots for GO terms generated from the Sham and TAC and heart RNA-Seq results of the Balb/cJ (cJ) and Balb/cByJ (cByJ) mice.

gene expression (Fig. 3). Meanwhile, H3K9Ac levels were minimally perturbed by the type of diet. Thus, to determine whether the higher H3K9Bu levels restricted stress-induced changes in gene expression, we examined the response of the ACADS-deficient mice vs wild-type mice to TAC-induced changes in gene expression.

Using the same dietary and surgical conditions described in Figure 6, we performed RNA-Seq to determine the associated changes in gene expression in the heart. We analyzed the relationship between ACADS, H3K9Bu, H3K9Ac, and gene expression in the unstressed and TAC-induced hearts by integrating the results of the ChIP—Seq (promoter regions) and RNA-Seq. The genes were then sorted according to those that were either significantly ($p \leq 0.05$) upregulated or downregulated in the Balb/cJ hearts post-TAC. These results revealed the global nature of the changes in H3K9Bu in the heart post-TAC, where it was downregulated in the wild-type mice but upregulated when ACADS was deleted as revealed by the medians and quartiles in the violin plots (Figure 7A,D). In contrast, H3K9Ac increased (~20%) post-TAC at the promoters of genes with upregulated RNA (Figure 7B). Notably, the ACADS-deficient mice had higher unstressed median levels of promoter-H3K9Ac, which also increased incrementally post-TAC to levels slightly higher than those observed in the wild-type mice. However, promoter-H3K9Ac was unchanged at the promoters of the downregulated genes in the wild-type mice but slightly reduced in the ACADS-deficient mice (Figure 7E). The RNA-Seq data revealed no major significant changes in the levels of gene expression in the unstressed hearts of the ACADS-deficient vs wild-type mice. However, TAC induced greater increases and decreases in gene expression in the latter as evident in the violin plots of the shrunken LFC and MA plots (Figure 7C—F,G and H and Supplementary Figure 12S). Enrichment plots of GO terms were generated from the RNA-Seq data. As examples, we show one GO term with upregulated genes GO basement membrane, and one term with downregulated genes GO respiratory chain complex (Figure 7I—J), both of which were relevant to the stressed heart. In both cases, the Balb/cJ vs cByJ/ΔACADS mice exhibited greater changes in gene expression (Figure 7I—J). At this time point (1 week post-TAC), TAC induced a significant increase in the left ventricular (LV) mass in the wild-type but did not reach significance in the ACADS-deficient mice, which was also associated with better cardiac functions (Supplementary Figure 1S). Thus, the data revealed that, similar to the mice on the fat-free vs high-fat diet, the mice with ΔACADS had higher promoter-H3K9Bu post-TAC that coincided with blunted changes in gene expression vs wild-type mice. Accordingly, we extrapolated from this that higher promoter-H3K9Bu may curb stress-induced changes in gene expression, but the mechanism remains unknown.

4. DISCUSSION

Although we know that acyl-CoA molecules such as butyryl- and crotonyl-CoA (intermediates of even-chain β-oxidation) or propionyl-CoA (intermediate of odd-chain β-oxidation) are required for histone modifications [11,35,36], we have no certain knowledge on how they are transported to the nucleus, as they cannot be exported from the mitochondria. We previously reported that β-oxidation enzymes, including acyl-CoA synthetase long-chain 1 (ACSL1), acyl-CoA dehydrogenase medium-chain (ACADM), acyl-CoA dehydrogenase long-chain (ACADL), ACAA2, HADHA, and HADHB are associated with H2A.Z-bound chromatin at active gene promoters [4]. This was serendipitously identified by an anti-H2A.Z rapid ChIP, followed by mass spectrometry of endogenous protein (RIME) [37] of heart chromatin. We confirmed this association using ACAA2 ChIP—Seq of heart chromatin. This is also corroborated by the fact that ACAA2 had a putative NLS, which we have shown to mediate its nuclear import [4]. We also show herein that HADHA and ACADS localized to the nucleus and that deletion of ACAA2 or HADHA reduced the abundance of H3K9Bu and H3K9Cr, whereas deletion of ACADS increased it significantly in human cells and the mouse heart (Figure 1 and Figure 5). We surmised that nuclear-localized β-oxidation enzymes catalyze fatty acids to generate short-chain acyl-CoA intermediates that could be used as histone modifiers. It should be noted that, alternatively, butyryl-CoA could be synthesized from butyrate (produced in the intestine by bacterial fermentation of non-digestible polysaccharides) via acyl-CoA synthetase short-chain family member 2 (ACSS2) in the nucleus [11]. However, our results demonstrate that this is not the only source of this substrate, as H3K9Bu abundance is not only modulated by deletions of β-oxidation enzymes, but also strongly regulated by dietary fat in an ACADS-regulated fashion *in vivo* and in cultured cells. This is an initial report of the genome-wide distribution of H3K9Bu in the mouse heart, where it is predominantly localized at the promoters of all of the expressed genes, and in a fraction of those, it extends throughout the gene body (Figure 6 and Supplementary Figure 11S). Moreover, we demonstrated how those levels are sensitive to diet and stress. Paradoxically, however, a high-fat vs fat-free diet had the lowest levels of H3K9Bu. We found that this could be explained by a significant increase in ACADS expression, together with other β-oxidation enzymes that were induced by the high-fat diet (Figure 3I—J), limiting the accumulation of any intermediates. This was supported by the reversal of high-fat-induced reduction of H3K9Bu in the ACADS-deficient mice (Figure 5B). Additionally, applying stress on the heart by transverse aortic constriction (TAC) reduced the levels of H3K9Bu in an ACADS-dependent manner, as deletion of the enzyme reversed this effect and, overall, increased H3K9Bu (Figures 5 and 6). Kebede et al. were the first to report the genome-wide distribution of H3K14Bu [36]. However, in their study, knockout of ACADS did not influence the abundance of this modification in mouse liver. Similarly, we observed that H3K18Bu was not influenced by the knockout of ACADS in the heart (Figure 5), suggesting that butyrylation of specific amino acid is highly regulated and not constitutively driven by an abundance of butyryl-CoA.

Since we established that H3K9Bu is regulated by ACADS, it was surprising to see it highest with a fat-free diet. A plausible explanation was that in the absence of fatty acids, carbohydrates are converted into fatty acid via FASN. Indeed, we confirmed this in ΔFASN cells, where H3K9Bu was barely detectable in the presence of glucose, whereas it was fully reconstituted in the presence of fatty acids (Figure 4). In contrast to H3K9Bu, the type of diet or gene knockouts applied in our study did not have a substantial effect on promoter-H3K9Ac. This was a reflection of the numerous confirmed sources of acetyl-CoA. On the one hand, during substrate abundance, citrate is exported from the mitochondria to the nucleus, where ACLY converts it into acetyl-CoA [1], so it can be equally sustained by dietary carb, protein, fat, or any metabolic substrate that converges on the TCA cycle. During substrate shortage, acetate is imported from the circulation and converted into acetyl-CoA by nuclear ACSS2 [38]. Moreover, others [2,3] and we [4] have uncovered the presence of pyruvate dehydrogenase complex in the nucleus, where it generates acetyl-CoA for histone acetylation [3]. Thus, with this wide spectrum of acetyl-CoA sources, it is hardly surprising that H3K9Ac is not substantially affected by diet.

An interesting aspect of our findings was the global nature of the genomic changes in H3K9Bu abundance with diet or stress (they did not correlate with specific changes in gene expression). In particular, the high-fat diet reduced genomic H3K9Bu by an average of 66% in all

of the peaks (Figures 2 and 3 and Supplementary Figure 4Sa). In the unstressed heart, the expression of 2,625 genes were significantly different in the mice on the high-fat vs fat-free diet (Supplementary Figure 7S). The majority of those (2,394 genes) increased, albeit very modestly (average increase = 1.1-fold). In contrast, major differences in gene expression in the high-fat vs fat-free diet became evident only after stress was applied to the heart; the extent of upregulation of RNA in TAC/Sham (shrunken LFC medians = 0.85 high-fat vs 0.55 fat-free diet) or downregulation (shrunken LFC medians = −0.6 high-fat vs - 0.3 fat-free diet) of gene expression was consistently greater with the high-fat diet, coinciding with the globally lower levels of H3K9Bu in the unstressed or stressed hearts (Figure 3). These results alone did not implicate the differences in H3K9Bu levels in the extent of changes in gene expression observed in the different diets. However, when compared with the Balb/cJ (wild-type) and cByJ (ΔACADS) mice, we were able to establish that link.

Similar to the mice models on different diets, the knockout of ACADS had a minimal impact on levels of gene expression in the unstressed heart (Supplementary Figure 7S). Differences were triggered only after stress, where the extent of upregulation of RNA in TAC/Sham (shrunken LFC with medians = 0.83 WT vs 0.51 ΔACADS) or downregulation (shrunken LFC with medians = −0.52 WT vs −0.29 ΔACADS) of gene expression was consistently greater in the wild-type vs ΔACADS mice. Thus, we extrapolated from this that the higher levels of H3K9Bu in the fat-free vs high-fat-fed mice and the ΔACADS vs WT mice after stress curbed the changes in gene expression. We predicted that the major global changes in H3K9Bu induced by diet or stress may have been responsible for regulating the recruitment of transcription factor(s), either directly or indirectly. It was also plausible that the reduction in H3K9Bu might have been associated with an increase in other histone marks, for example, crotonyl, which remains to be explored under these conditions.

The debate continues regarding how fatty acid- vs carbohydrate-rich diets impacts cardiovascular health [39,40]. This study is the first demonstration of how a high-fat vs a low-fat or fat-free diet impacts the histone code by substantially reducing H3K9Bu in a genome-wide fashion. Interestingly, within a short period (11 days), a high-fat diet appears to have no adverse effects on cardiac function under quiescent/unstressed conditions. It is, though, associated with modest, significant, increases in the expression of β-oxidation enzymes, as it adapts to the high-fat diet by accelerating its metabolism, which explains the decrease in histone butyrylation (Figure 3l). Notably, the impact of diet on the heart became more evident when stress was imposed via work overload. In this case, our data revealed that high-fat was associated with more pronounced changes in gene expression, whether it was upregulation or downregulation. In particular, one of the most detrimental changes in the heart was the significant reduction in the respiratory complex proteins with the high- vs low-fat diet only after stress was applied (Fig. 3o). The greater changes in gene expression coincided with reduced levels of H3K9Bu associated with the high-fat diet (Figures 2 and 3A–F), which is reversed by deletion/inhibition of ACADS. Thus, our results confirmed and partly explained the adverse effect of a high-fat diet on cardiovascular health, especially during stress, and its relation to the underlying epigenetics. The findings provide an incremental first step in understanding the impact of diet on the heart's epigenetics, which would eventually afford us the knowledge to manipulate it to our advantage.

5. ACCESSION NUMBERS

The ChIP-Seq and RNA-Seq data files were grouped into five datasets that were deposited in GEO with the following, publically available, accession number: GSE165279, GSE165271, GSE165236, GSE165085, and GSE165284.

FUNDING

This study was supported by the National Institute of Health award, R01 HL146537, to M.A.

ACKNOWLEDGMENTS

We thank Dr. Junichi Sadoshima, Chairman of the Department of Cell Biology and Molecular Medicine, Rutgers University, for his support.

CONFLICT OF INTEREST

The authors declare that they have no conflicts of interest with this article's content. The content is solely the responsibility of the authors and does not necessarily represent the official views of the National Institutes of Health.

APPENDIX A. SUPPLEMENTARY DATA

Supplementary data to this article can be found online at https://doi.org/10.1016/j.molmet.2021.101249.

AUTHOR CONTRIBUTIONS

Zhi Yang: Mice surgery, echocardiography, and Western blotting analysis. Minzhen He: Tissue and cell culturing, vector construction, and measurements of oxygen consumption rates. Julianne Austin: Cell culturing and Western blotting analysis. Jessica Pfleger: Data analysis. Maha Abdellatif: Conceptualization, design, data analysis, produced the figures, and writing.

REFERENCES

[1] Wellen, K.E., Hatzivassiliou, G., Sachdeva, U.M., Bui, T.V., Cross, J.R., Thompson, C.B., 2009. ATP-citrate lyase links cellular metabolism to histone acetylation. Science 324(5930):1076—1080. https://doi.org/10.1126/science.1164097.

[2] Sutendra, G., Kinnaird, A., Dromparis, P., Paulin, R., Stenson, T.H., Haromy, A., et al., 2014. A nuclear pyruvate dehydrogenase complex is important for the generation of acetyl-CoA and histone acetylation. Cell 158(1):84—97. https://doi.org/10.1016/j.cell.2014.1004.1046.

[3] Nagaraj, R., Sharpley, M.S., Chi, F., Braas, D., Zhou, Y., Kim, R., et al., 2017. Nuclear localization of mitochondrial TCA cycle enzymes as a critical step in mammalian zygotic genome activation. e211 Cell 168(1—2):210—223. https://doi.org/10.1016/j.cell.2016.10.12. Epub 2017 Jan 1012.

[4] Choi, S., Pfleger, J., Jeon, Y.H., Yang, Z., He, M., Shin, H., et al., 2019. Oxoglutarate dehydrogenase and acetyl-CoA acyltransferase 2 selectively associate with H2A.Z-occupied promoters and are required for histone modifications. Biochimica Biophysics Acta General Regulation Mechanica 1862(10):194436. https://doi.org/10.1016/j.bbagrm.2019.194436. Epub 192019 Nov 194431.

[5] Wang, Y., Guo, Y.R., Liu, K., Yin, Z., Liu, R., Xia, Y., et al., 2017. KAT2A coupled with the alpha-KGDH complex acts as a histone H3 succinyltransferase. Nature 552(7684):273—277, 210.1038/nature25003. Epub 22017 Dec 25006.

[6] Javaid, N., Choi, S., 2017. Acetylation- and methylation-related epigenetic proteins in the context of their targets. Genes 8(8):196. https://doi.org/10.3390/genes8080196.

[7] Chen, Y., Sprung, R., Tang, Y., Ball, H., Sangras, B., Kim, S.C., et al., 2007. Lysine propionylation and butyrylation are novel post-translational

modifications in histones. Molecular & Cellular Proteomics 6(5):812–819. https://doi.org/10.1074/mcp.M700021-MCP700200. Epub 702007 Jan 700030.

[8] Goudarzi, A., Zhang, D., Huang, H., Barral, S., Kwon, O.K., Qi, S., et al., 2016. Dynamic competing histone H4 K5K8 acetylation and butyrylation are hallmarks of highly active gene promoters. Molecular Cell 62(2):169–180. https://doi.org/10.1016/j.molcel.2016.1003.1014.

[9] Goudarzi, A., Hosseinmardi, N., Salami, S., Mehdikhani, F., Derakhshan, S., Aminishakib, P., 2020. Starvation promotes histone lysine butyrylation in the liver of male but not female mice. Gene 745:144647. https://doi.org/10.1016/j.gene.2020.144647. Epub 142020 Apr 144642.

[10] Nie, L., Shuai, L., Zhu, M., Liu, P., Xie, Z.F., Jiang, S., et al., 2017. The landscape of histone modifications in a high-fat diet-induced obese (DIO) mouse model. Molecular & Cellular Proteomics 16(7):1324–1334. https://doi.org/10.1074/mcp.M1117.067553. Epub 062017 Apr 067527.

[11] Sabari, B.R., Zhang, D., Allis, C.D., Zhao, Y., 2017. Metabolic regulation of gene expression through histone acylations. Nature Reviews Molecular Cell Biology 18(2):90–101. https://doi.org/10.1038/nrm.2016.1140. Epub 2016 Dec 1037.

[12] Houten, S.M., Violante, S., Ventura, F.V., Wanders, R.J., 2016. The biochemistry and physiology of mitochondrial fatty acid β-oxidation and its genetic disorders. Annual Review of Physiology 78:23–44. https://doi.org/10.1146/annurev-physiol-021115-105045. Epub 022015 Oct 021114.

[13] Lennarz, W.J., Light, R.J., Bloch, K., 1962. A fatty acid synthetase from E. Coli. Proceedings of the National Academy of Sciences of the United States of America 48(5):840–846. https://doi.org/10.1073/pnas.1048.1075.1840.

[14] Sayed, D., Yang, Z., He, M., Pfleger, J., Abdellatif, M., 2015. Acute targeting of general transcription factor IIB restricts cardiac hypertrophy via selective inhibition of gene transcription. Circ HF 8(1):138–148.

[15] Chen, I.Y., Lypowy, J., Pain, J., Sayed, D., Grinberg, S., Alcendor, R.R., et al., 2006. Histone H2A.z is essential for cardiac myocyte hypertrophy but opposed by silent information regulator 2alpha. Journal of Biological Chemistry 281(28):19369–19377.

[16] Lypowy, J., Chen, I.Y., Abdellatif, M., 2005. An alliance between Ras GTPase-activating protein, filamin C, and Ras GTPase-activating protein SH3 domain-binding protein regulates myocyte growth. Journal of Biological Chemistry 280(27):25717–25728.

[17] Rane, S., He, M., Sayed, D., Vashistha, H., Malhotra, A., Sadoshima, J., et al., 2009. Downregulation of MiR-199a derepresses hypoxia-inducible factor-1 {alpha} and sirtuin 1 and recapitulates hypoxia preconditioning in cardiac myocytes. Circulation Research 104(7):879–886.

[18] Jeon, Y.H., He, M., Austin, J., Shin, H., Pfleger, J., Abdellatif, M., 2021. Adiponectin enhances the bioenergetics of cardiac myocytes via an AMPK- and succinate dehydrogenase-dependent mechanism. Cellular Signalling 78:109866. https://doi.org/10.1016/j.cellsig.2020.109866. Epub 102020 Dec 109861.

[19] Pfleger, J., He, M., Abdellatif, M., 2015. Mitochondrial complex II is a source of the reserve respiratory capacity that is regulated by metabolic sensors and promotes cell survival. Cell Death & Disease 6:e1835.

[20] Han, M., Yang, Z., Sayed, D., He, M., Gao, S., Lin, L., et al., 2012. GATA4 expression is primarily regulated via a miR-26b-dependent posttranscriptional mechanism during cardiac hypertrophy. Cardiovascular Research 93(4):645–654.

[21] Sayed, D., Hong, C., Chen, I.Y., Lypowy, J., Abdellatif, M., 2007. MicroRNAs play an essential role in the development of cardiac hypertrophy. Circulation Research 100(3):416–424.

[22] Zhang, Y., Liu, T., Meyer, C.A., Eeckhoute, J., Johnson, D.S., Bernstein, B.E., et al., 2008. Model-based analysis of ChIP-seq (MACS). Genome Biology 9(9):R137. https://doi.org/10.1186/gb-2008-1189-1189-r1137. Epub 2008 Sep 1117.

[23] Liao, Y., Smyth, G.K., Shi, W., 2014. featureCounts: an efficient general purpose program for assigning sequence reads to genomic features. Bioinformatics 30(7):923–930.

[24] Love, M.I., Huber, W., Anders, S., 2014. Moderated estimation of fold change and dispersion for RNA-seq data with DESeq2. Genome Biology 15(12):550.

[25] Nicol, J.W., Helt, G.A., Blanchard Jr., S.G., Raja, A., Loraine, A.E., 2009. The Integrated Genome Browser: free software for distribution and exploration of genome-scale datasets. Bioinformatics 25(20):2730–2731.

[26] Lerdrup, M., Johansen, J.V., Agrawal-Singh, S., Hansen, K., 2016. An interactive environment for agile analysis and visualization of ChIP-sequencing data. Nature Structural & Molecular Biology 23(4):349–357. https://doi.org/10.1038/nsmb.3180. Epub 2016 Feb 1029.

[27] Mootha, V.K., Lindgren, C.M., Eriksson, K.-F., Subramanian, A., Sihag, S., Lehar, J., et al., 2003. PGC-1α-responsive genes involved in oxidative phosphorylation are coordinately downregulated in human diabetes. Nature Genetics 34(3):267–273.

[28] Subramanian, A., Tamayo, P., Mootha, V.K., Mukherjee, S., Ebert, B.L., Gillette, M.A., et al., 2005. Gene set enrichment analysis: a knowledge-based approach for interpreting genome-wide expression profiles. Proceedings of the National Academy of Sciences 102(43):15545–15550.

[29] Landt, S.G., Marinov, G.K., Kundaje, A., Kheradpour, P., Pauli, F., Batzoglou, S., et al., 2012. ChIP-seq guidelines and practices of the ENCODE and modENCODE consortia. Genome Research 22(9):1813–1831. https://doi.org/10.1101/gr.136184.136111.

[30] Waterson, R.M., Hill, R.L., 1972. Enoyl coenzyme A hydratase (crotonase). Catalytic properties of crotonase and its possible regulatory role in fatty acid oxidation. Journal of Biological Chemistry 247(16):5258–5265.

[31] Sayed, D., He, M., Yang, Z., Lin, L., Abdellatif, M., 2013. Transcriptional regulation patterns revealed by high resolution chromatin immunoprecipitation during cardiac hypertrophy. Journal of Biological Chemistry 288(4):2546–2558. https://doi.org/10.1074/jbc.M2112.429449. Epub 422012 Dec 429410.

[32] Chirala, S.S., Wakil, S.J., 2004. Structure and function of animal fatty acid synthase. Lipids 39(11):1045–1053. https://doi.org/10.1007/s11745-11004-11329-11749.

[33] Uhlen, M., Fagerberg, L., Hallstrom, B.M., Lindskog, C., Oksvold, P., Mardinoglu, A., et al., 2015. Proteomics. Tissue-based map of the human proteome. Science 347(6220):1260419. https://doi.org/10.1261126/science.1260419.

[34] Reue, K., Cohen, R.D., 1996. Acads gene deletion in BALB/cByJ mouse strain occurred after 1981 and is not present in BALB/cByJ-fld mutant mice. Mammalian Genome 7(9):694–695. https://doi.org/10.1007/s003359900208.

[35] Janke, R., Dodson, A.E., Rine, J., 2015. Metabolism and epigenetics. Annual Review of Cell and Developmental Biology 31:473–496. https://doi.org/10.1146/annurev-cellbio-100814-125544. Epub 102015 Sep 100810.

[36] Kebede, A.F., Nieborak, A., Shahidian, L.Z., Le Gras, S., Richter, F., Gómez, D.A., et al., 2017. Histone propionylation is a mark of active chromatin. Nature Structural & Molecular Biology 24(12):1048–1056. https://doi.org/10.1038/nsmb.3490. Epub 2017 Oct 1023.

[37] Mohammed, H., Taylor, C., Brown, G.D., Papachristou, E.K., Carroll, J.S., D'Santos, C.S., 2016. Rapid immunoprecipitation mass spectrometry of endogenous proteins (RIME) for analysis of chromatin complexes. Nature Protocols 11(2):316–326. https://doi.org/10.1038/nprot.2016.1020. Epub 2016 Jan 1021.

[38] Yoshii, Y., Furukawa, T., Yoshii, H., Mori, T., Kiyono, Y., Waki, A., et al., 2009. Cytosolic acetyl-CoA synthetase affected tumor cell survival under hypoxia: the possible function in tumor acetyl-CoA/acetate metabolism. Cancer Science 100(5):821–827.

[39] Diamond, D.M., O'Neill, B.J., Volek, J.S., 2020. Low carbohydrate diet: are concerns with saturated fat, lipids, and cardiovascular disease risk justified? Current Opinion in Endocrinology Diabetes and Obesity 27(5):291–300 https://doi.org/10.1097/MED.0000000000000568.

[40] Visioli, F., Poli, A., 2020. Fatty acids and cardiovascular risk. Evidence, lack of evidence, and diligence. Nutrients 12(12):3782. https://doi.org/10.3390/nu12123782.

